1991 CEDAR Workshop

NIST Auditorium, Boulder, CO

2-5PM Tuesday, June 18, 1991

Optics Short Course

Roger Smith et al.

University of Alaska at Fairbanks

Optics Tutorial

(Featuring Hernandez, Romick and Smith)

Tuesday Afternoon
NIST Auditorium 2.00pm - 5.00pm
4 Sessions starting at:-
2.00pm: Optics in Aeronomy
3.00pm: Imaging the atmosphere
3.45pm: Observing lines and bands
4.30pm: Doing dynamics optically.

The View of a Ground Based Instrument

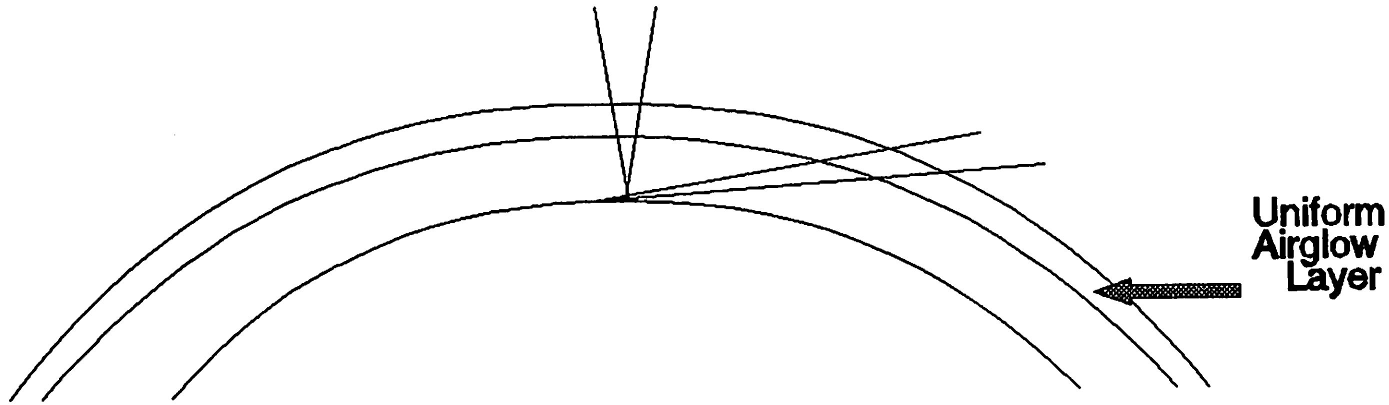

The van-Rhijn Effect

Meridian Scan Mode

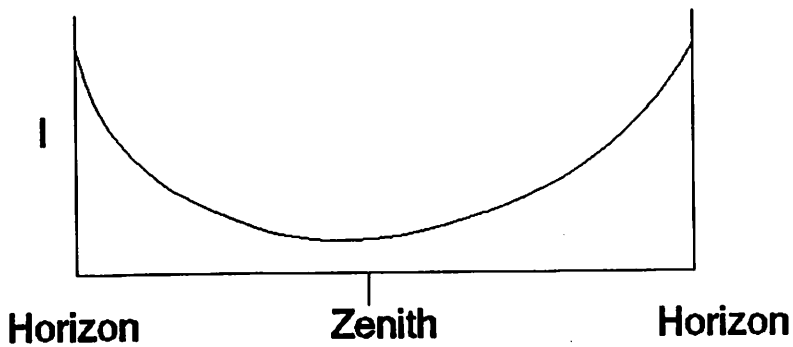

Alt-Azimuth Scan

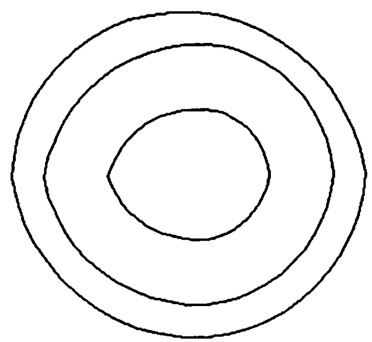

Isophote map

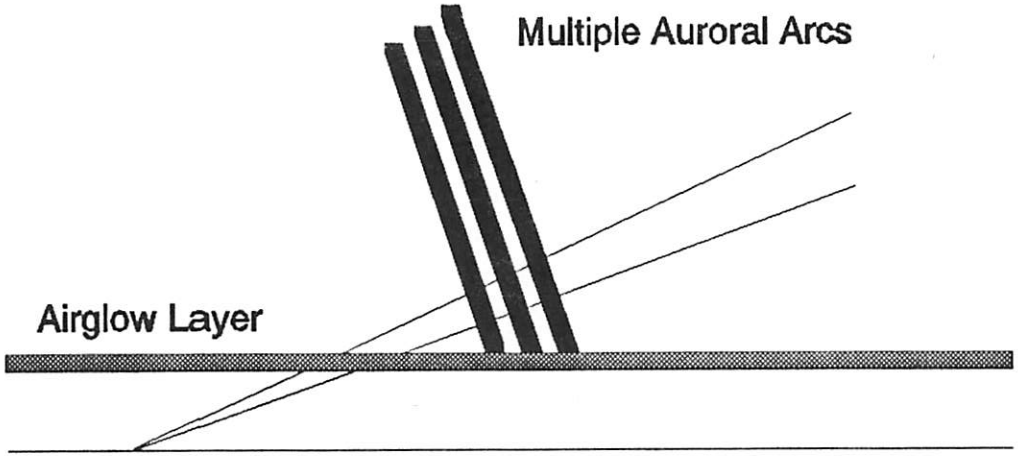

Ground-based view
of
Auroral Green Line

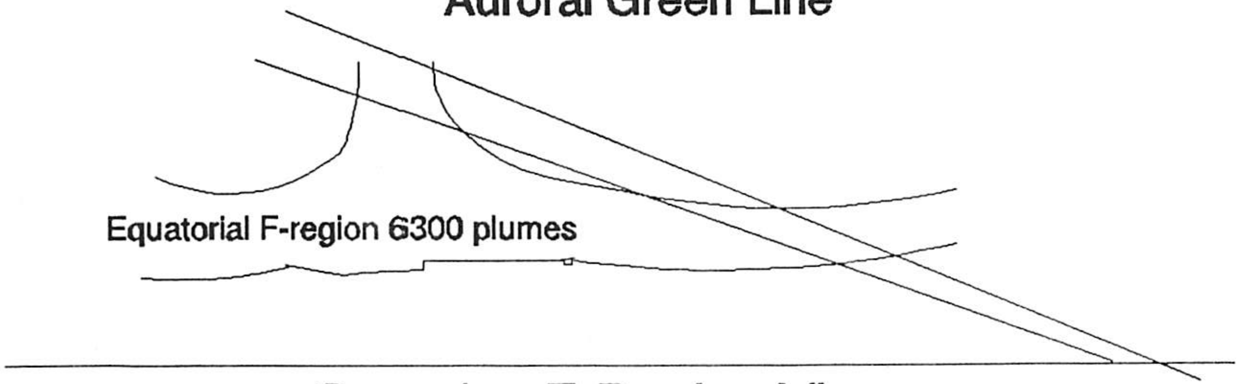

Complex F-Region View

Imaging the airglow layer

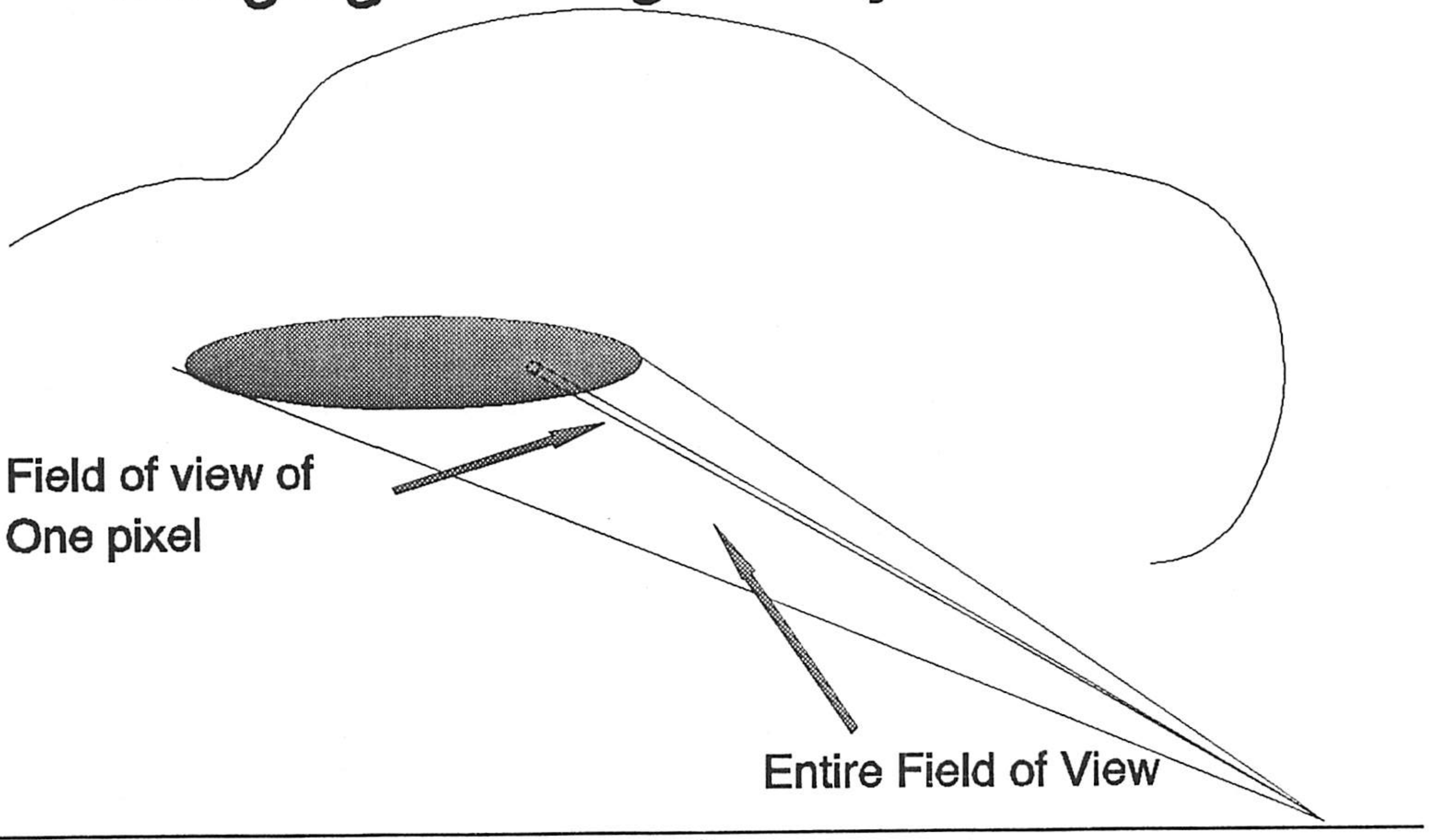

Signal seen = $\frac{A\Omega}{4\pi}$ R x 10^{6} Photons per second

Small pixels receive a weak signal, require more time.

Possible Interpretations of Varying Intensity

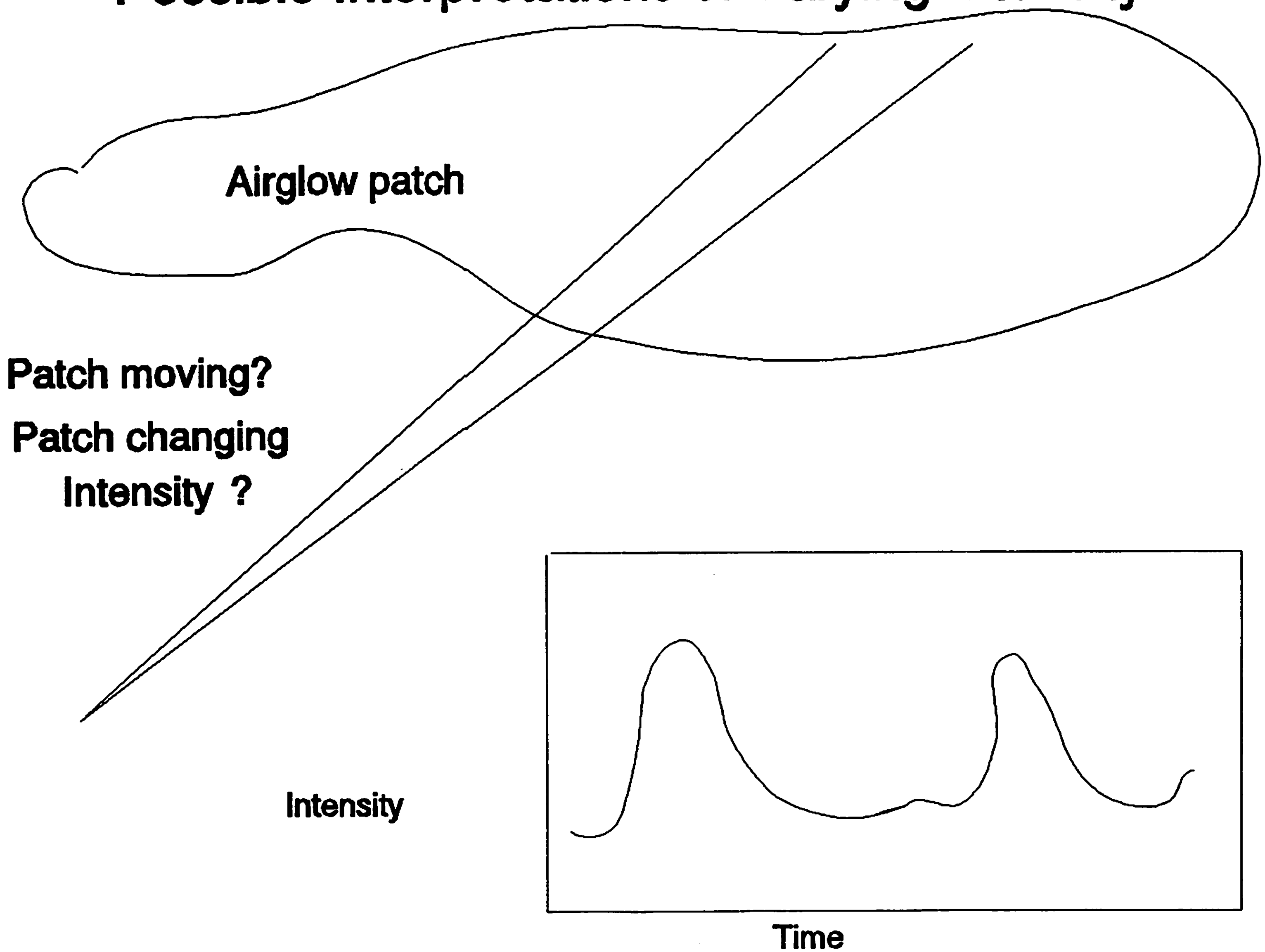

Observations with a Medium Resolution Spectrometer

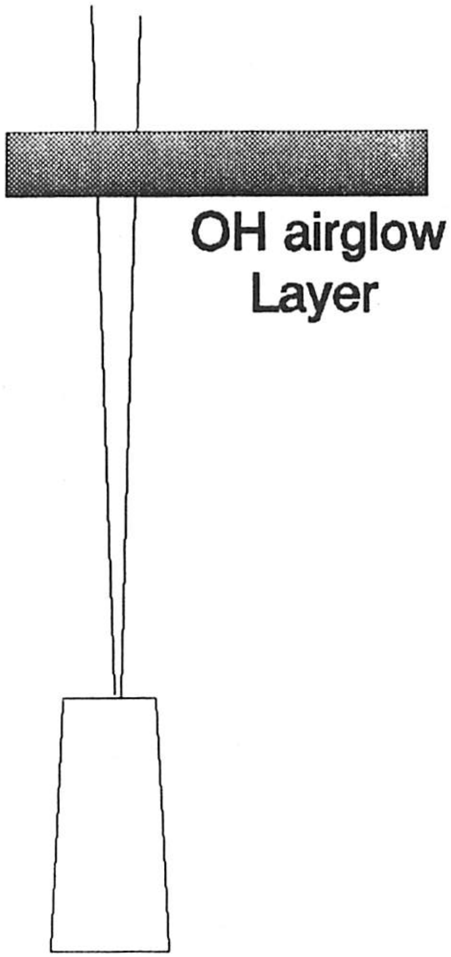

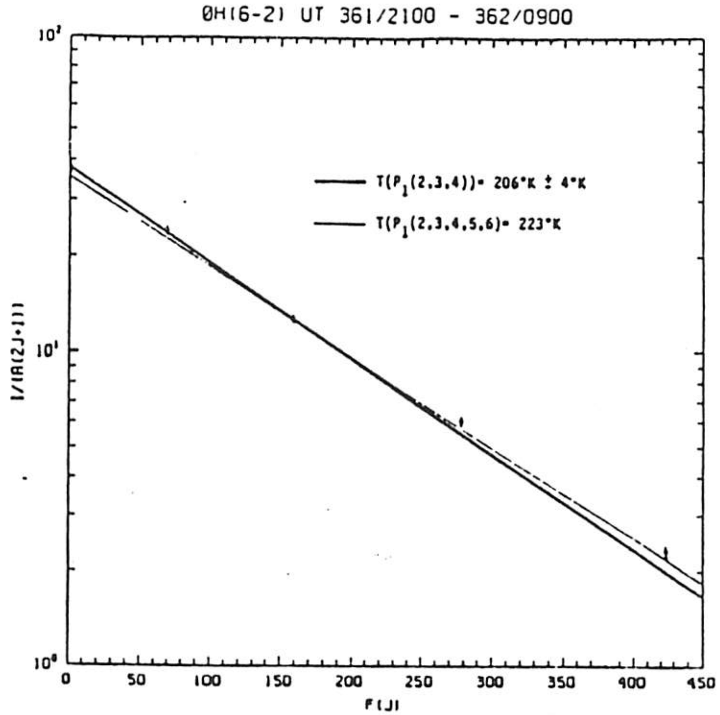

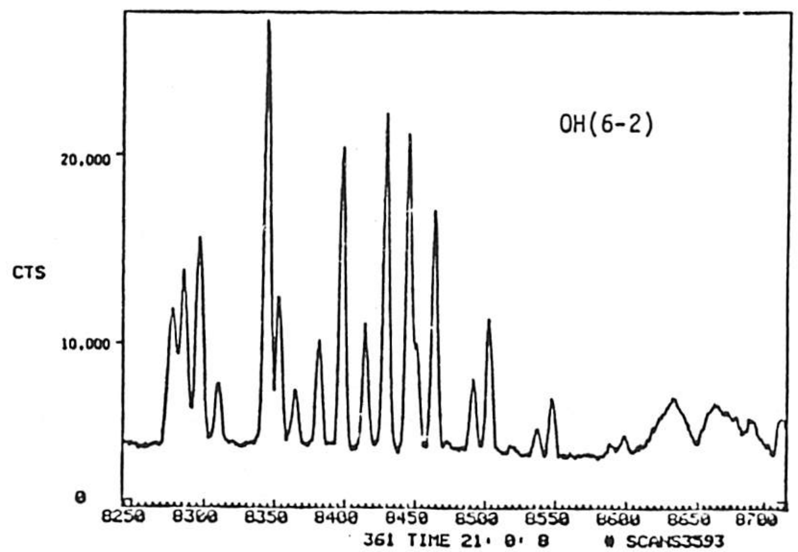

51-105

Observing Geometry

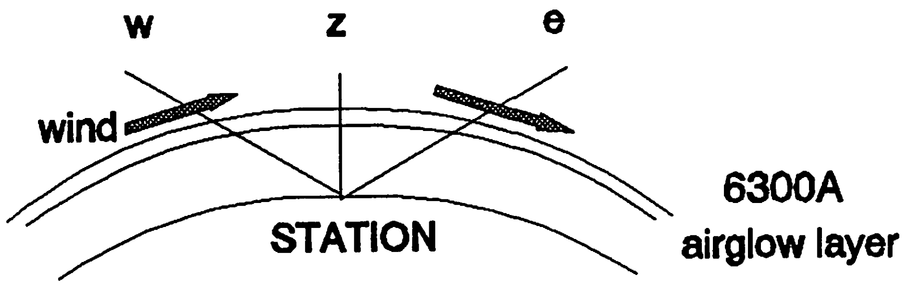

Observed Spectra
from a Fabry-Perot Spectrometer

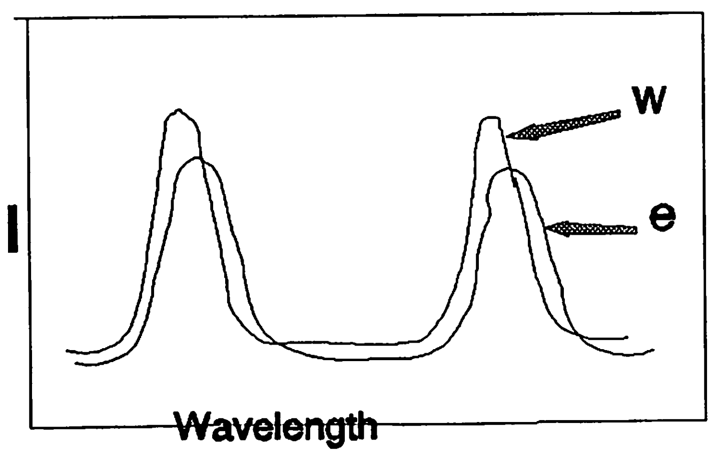

Dynamics Data
(for each direction of view)

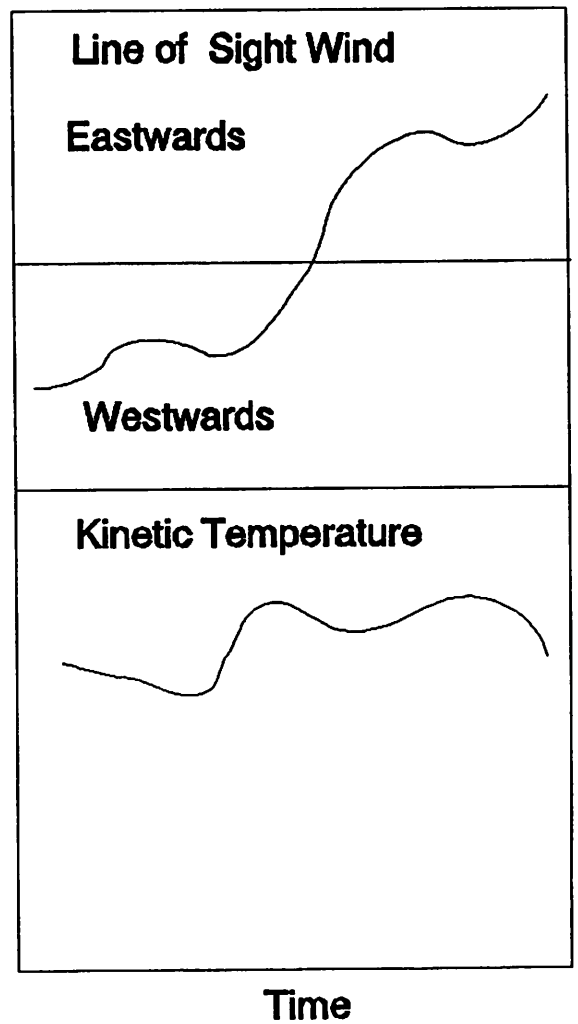

Observing Geometry

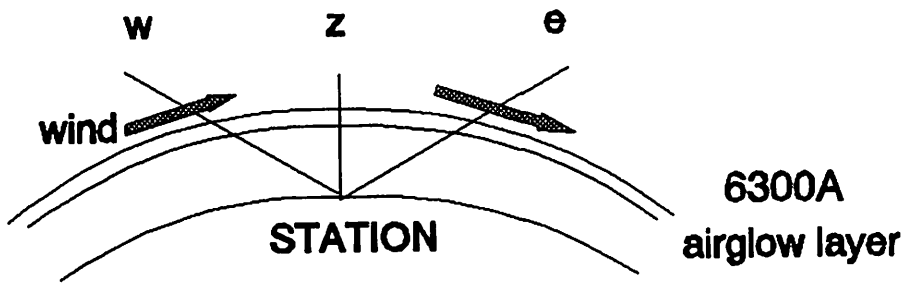

Observed Spectra
for a Michelson Interferometer
similar to a WAMDII

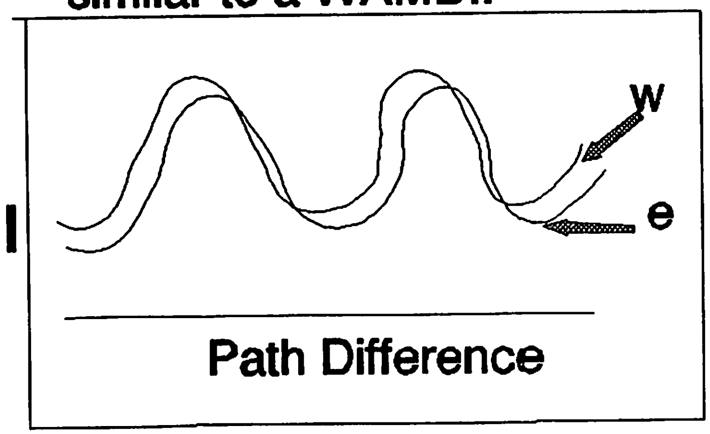

Dynamics Data
for each pixel in fringe image

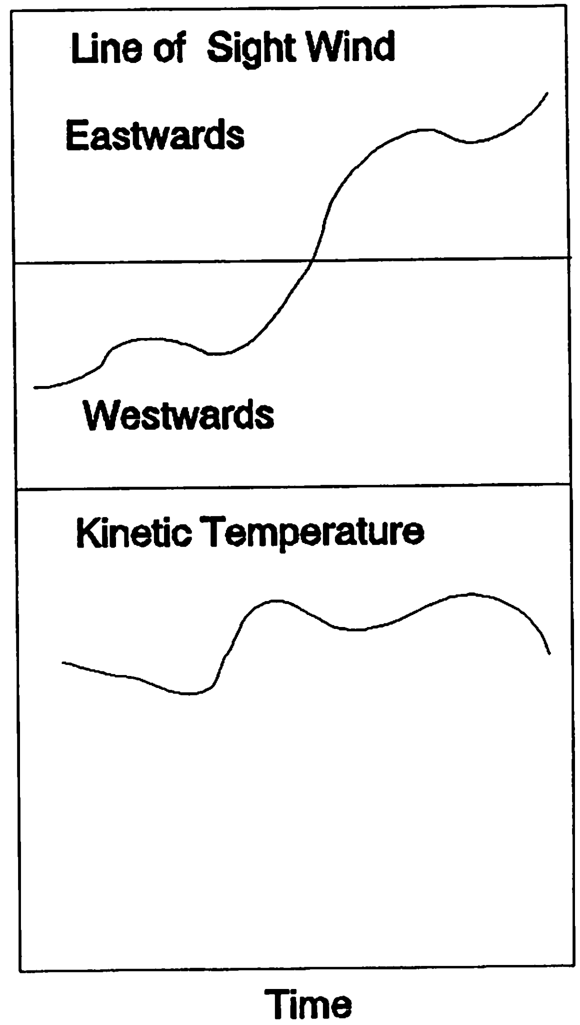

SI-10899

Wavelength Resolved Emissions can be used to identify the particular radiating atom or molecule. Other conditions lead to information about the excitation process.

Identification of the Emitter Through

ATMOSPHERIC RADIATION PROCESSES

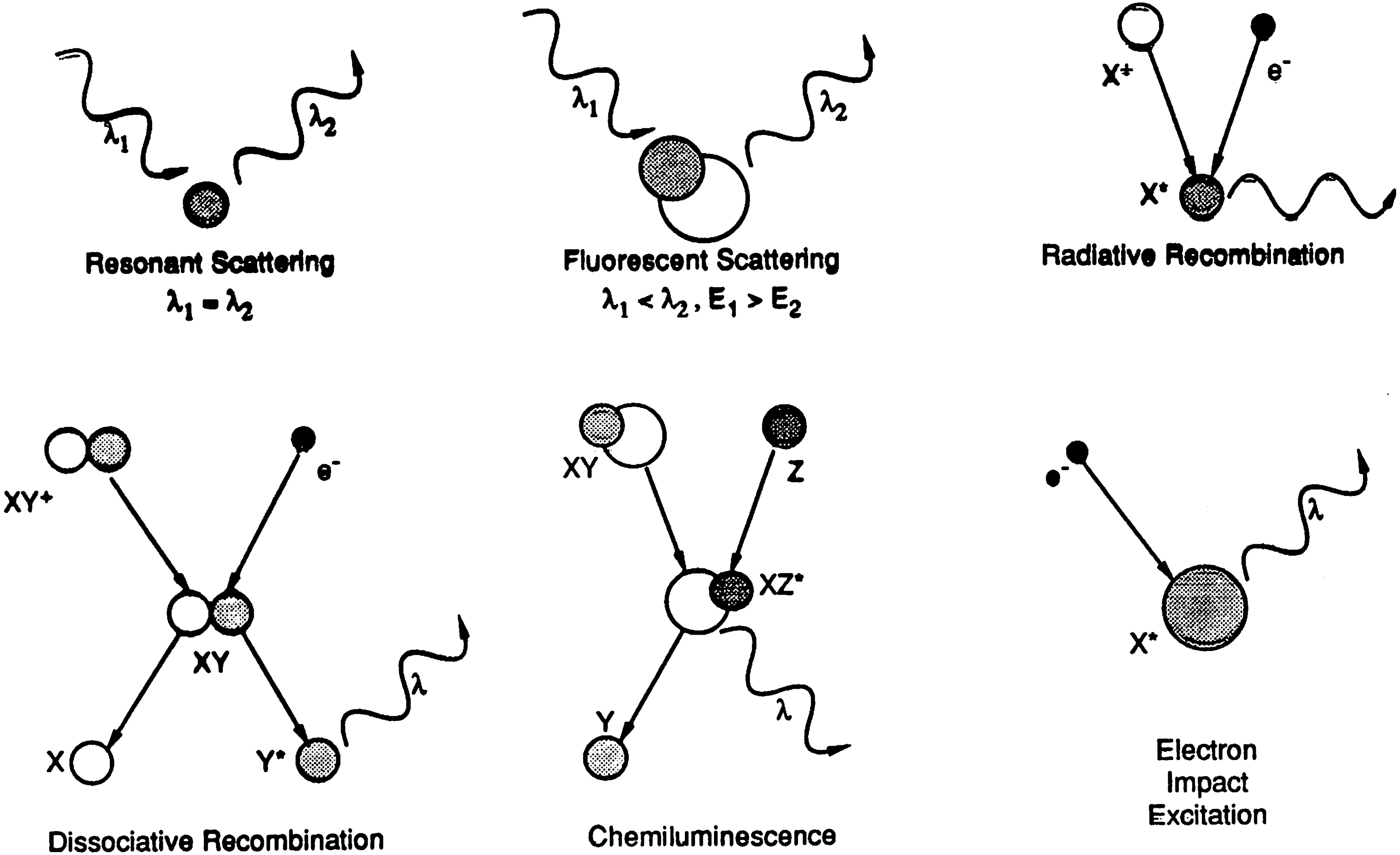

Excitation Conditions	Basic Process
Dayglow	Solar EUV and Photoelectrons
Twilight	Mixture - decay processes and chemistry - Conjugate photoelec.
Nightglow	Chemistry and conjugate photoelectrons
Aurora	All types of energetic particles

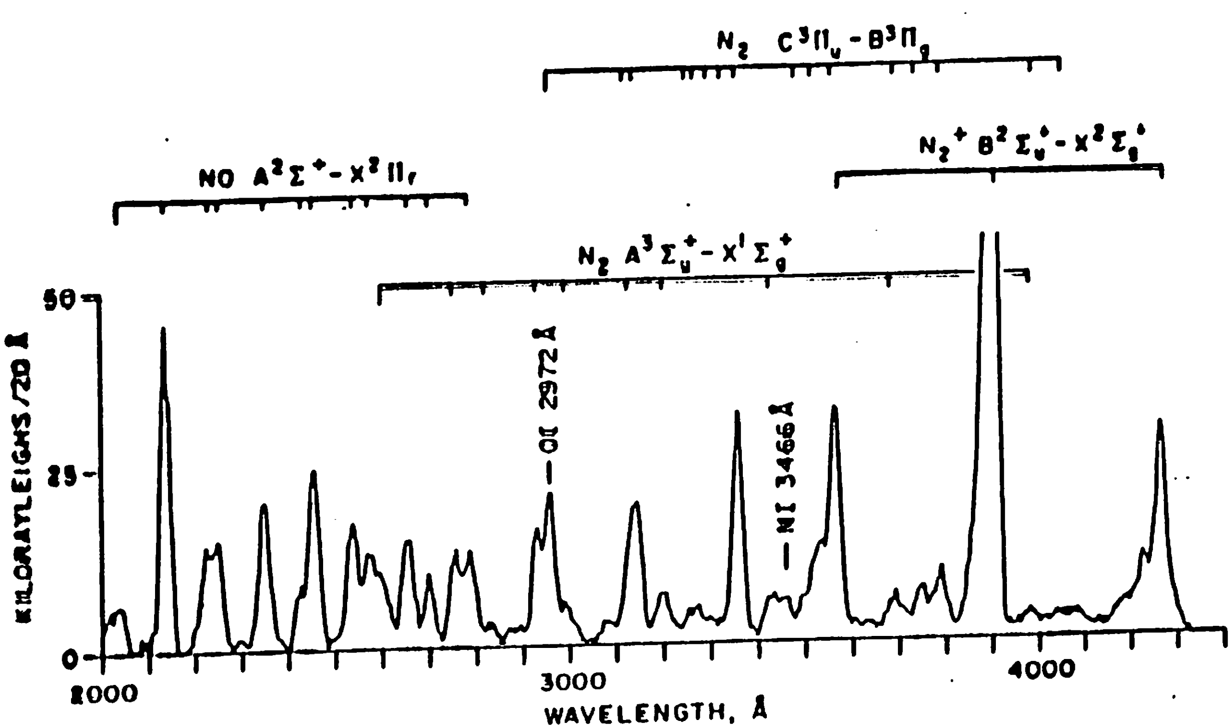

N_2 $C^3\Pi_u - B^3\Pi_g$
N_2^+ $B^2\Sigma_u^+ - X^2\Sigma_g^+$
NO $A^2\Sigma^+ - X^2\Pi_r$
N_2 $A^3\Sigma_u^+ - X^1\Sigma_g^+$
OII 2972 Å
NI 3466 Å
KILORAYLEIGHS/20 Å
50
25
0
2000
3000
4000
WAVELENGTH, Å

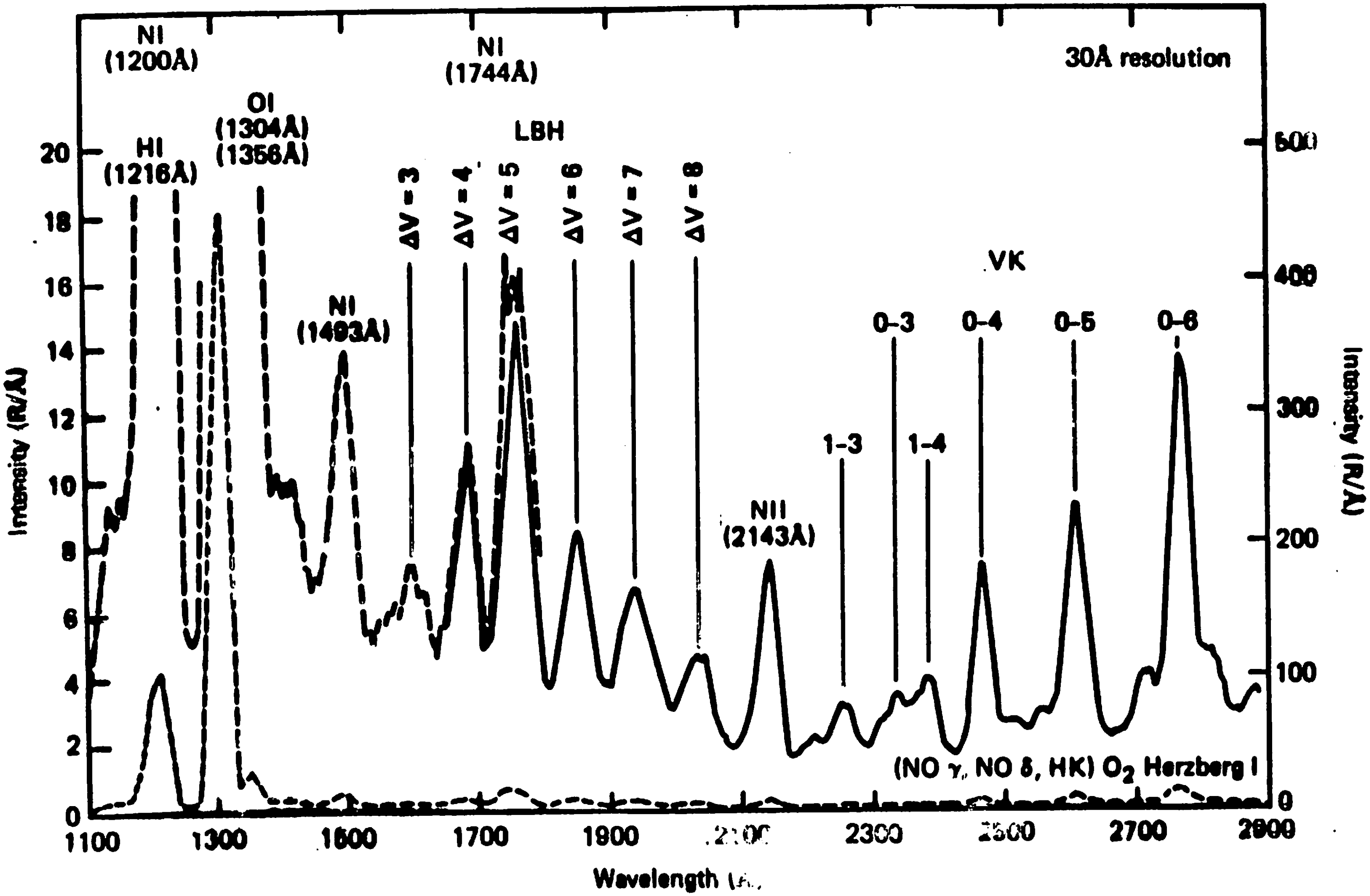
30Å resolution
NI (1200Å)
HI (1216Å)
OI (1304Å) (1356Å)
NI (1493Å)
NI (1744Å)
LBH
ΔV = 3
ΔV = 4
ΔV = 5
ΔV = 6
ΔV = 7
ΔV = 8
NII (2143Å)
VK
0-3
0-4
0-5
0-6
1-3
1-4
(NO γ, NO δ, HK) O2 Herzberg I
Intensity (R/Å)
Wavelength (Å)
0
2
4
6
8
10
12
14
16
18
20
100
200
300
400
500
1100
1300
1500
1700
1900
2100
2300
2500
2700
2900

Objective	Observable	Approach	Mode
Neutral Composition			
-Day atomic O	OI 130.4, 164.1 nm	Line ratios	E,L
	OI 130.4, 135.6 nm	Line ratios	E,L
	N_2 VK bands	Quenching	L
-Day N_2	N_2 LBH, 2PG bands	Emission peak	E,L
-Day O_2	N_2 LBH bands	Absorption O_2 SR	E,L
-Night O	O_2 Herzberg I	O+O	E,L
-Global dynamics	He 58.4 nm	He density	L
-Air density	Rayleigh scattering	Limb scans	L
Ionization rates			
-O+hν,e	OII 83.4, 61.7 nm	Rate from intensity	L
-N2+hν,e	NII 108.5, 91.6 nm	Rate from intensity	L
Photoelectron fluxes	N_2 LBH, 2PG	Combine with model	E,L
Minor species			
-Day NO	NO γ 215 nm	Fluorescent scattering	E,L
-Day N	NI 149.3, 174.3 nm	Electron impact	L
-Day Mg	MgI,II 285.2, 279.8 nm	Resonant scattering	L
-Day/night H	HI 121.6,102.6,656.3 nm	Resonant scattering	E,L
-Day He	HeI 58.4 nm	Resonant scattering	L
-Night N	NO δ bands	N+O	E,L
-Night NO	NO_2 continuum	N+O	E,L

E= Earth-viewing spectrographic imager makes measurement
L= Limb-viewing imaging spectrograph makes measurement

Objective	Observable	Approach	Mode
Electron density			
-Day	OII 83.4 nm	multiple scattering	L
-Day	OII 61.7,54.0 nm	line ratios	L
-Day/Storm	OI 135.6 nm, N_2 LBH	N_e from O/N_2 radtio	E
-Night	OI 91.1,130.4,135.6 nm	$O^+ + e$	L
-Night	OI 630 nm	$O_2^+ + e$	E,L
-F layer height	OI 130.4,135.6,630 nm	Hgt from line ratios	E,L
Gravity waves and Wave number spectra	OH (6,2) 825-860 nm	line ratio and spatial variations	E,L
	OH Meinel		E,L
	O_2 ATM		E,L
	OI 557.7 nm		E

Objective	Observable	Approach	Mode
Polar mesosph clouds	ice	Mie scattering	E,L
Auroras	all bands	Particle precipitation	E,L
Energy deposition			
-Electrons	N_2 2PG, LBH; N_2^+ 1NG	Electron impact	E,L
	OI 297.2,557.7,630 nm	Electron impact	E
	OI 844.6 nm	Electron impact	E
-Protons	HI 121.6,486.1 nm	Proton impact	E
-Solar EUV	Dayglow	Photoelec. production	L
Neutral temperatures			
-Day	O_2 ATM	Band profile	E,L
	OI 135.6 nm, N_2 LBH,2PG	Scale height	L
-Night	OH Meinel, O_2 ATM	Band profile	E,L

There are very few cases where there is a simple direct relationship between a particular emission and the density of the emitter. Thus models enter as necessary linkages between observed emissions and derived parameters.

There are some studies that do not need quantitative intensity measurements or derived constituent densities. Morphological studies from images have contributed a great deal towards our understanding of the auroral oval.

POLAR BEAR AURORAL IMAGE

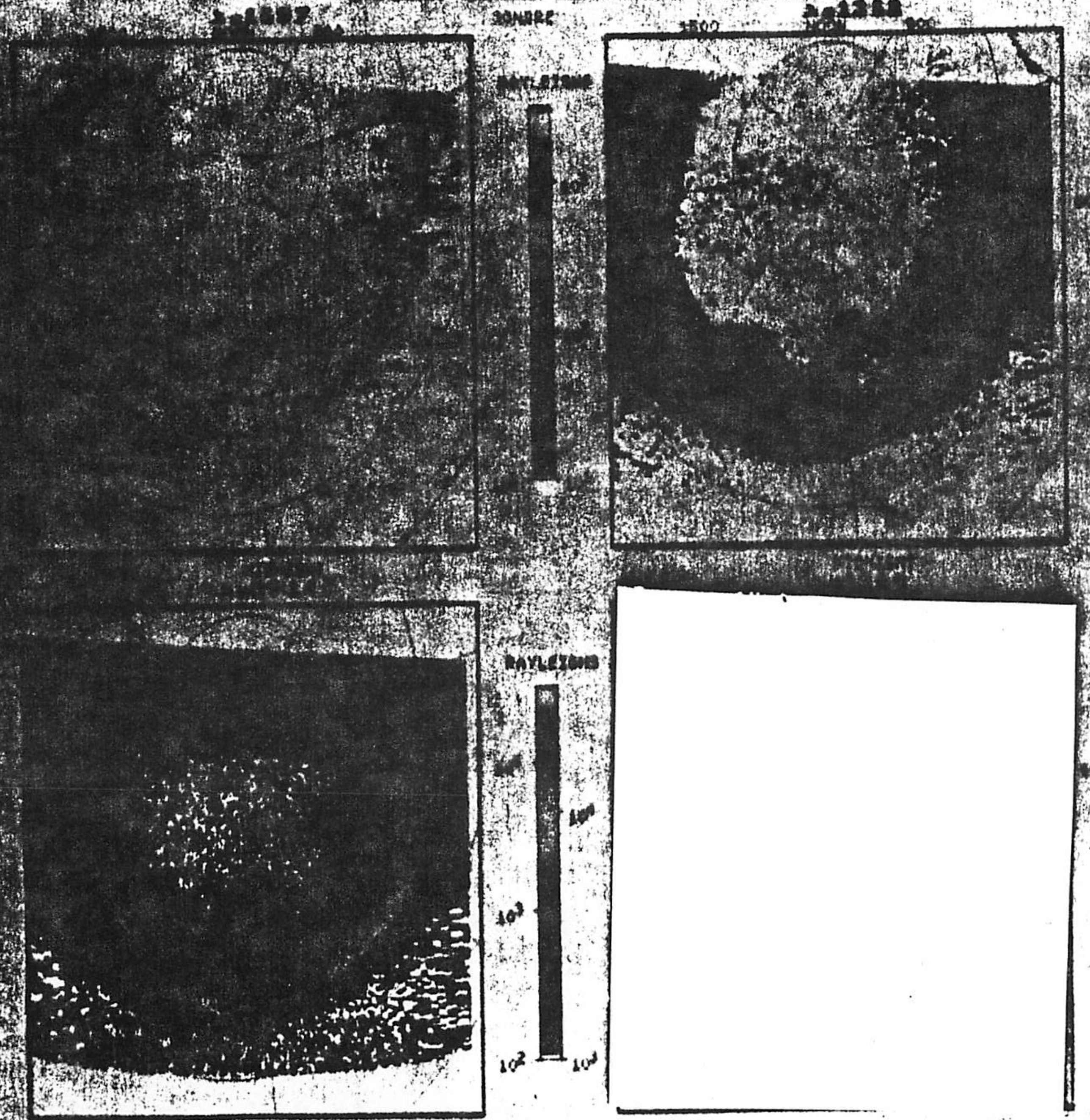

28 JAN 1987 (DAY 28) 4: 5:38 - 4:16:58

To cover all of the quantitative studies using optical observations is beyond the scope of this short course.

As examples I will concentrate on some DAYGlow observations and derived quantities.

EARTH ULTRAVIOLET SPECTRUM

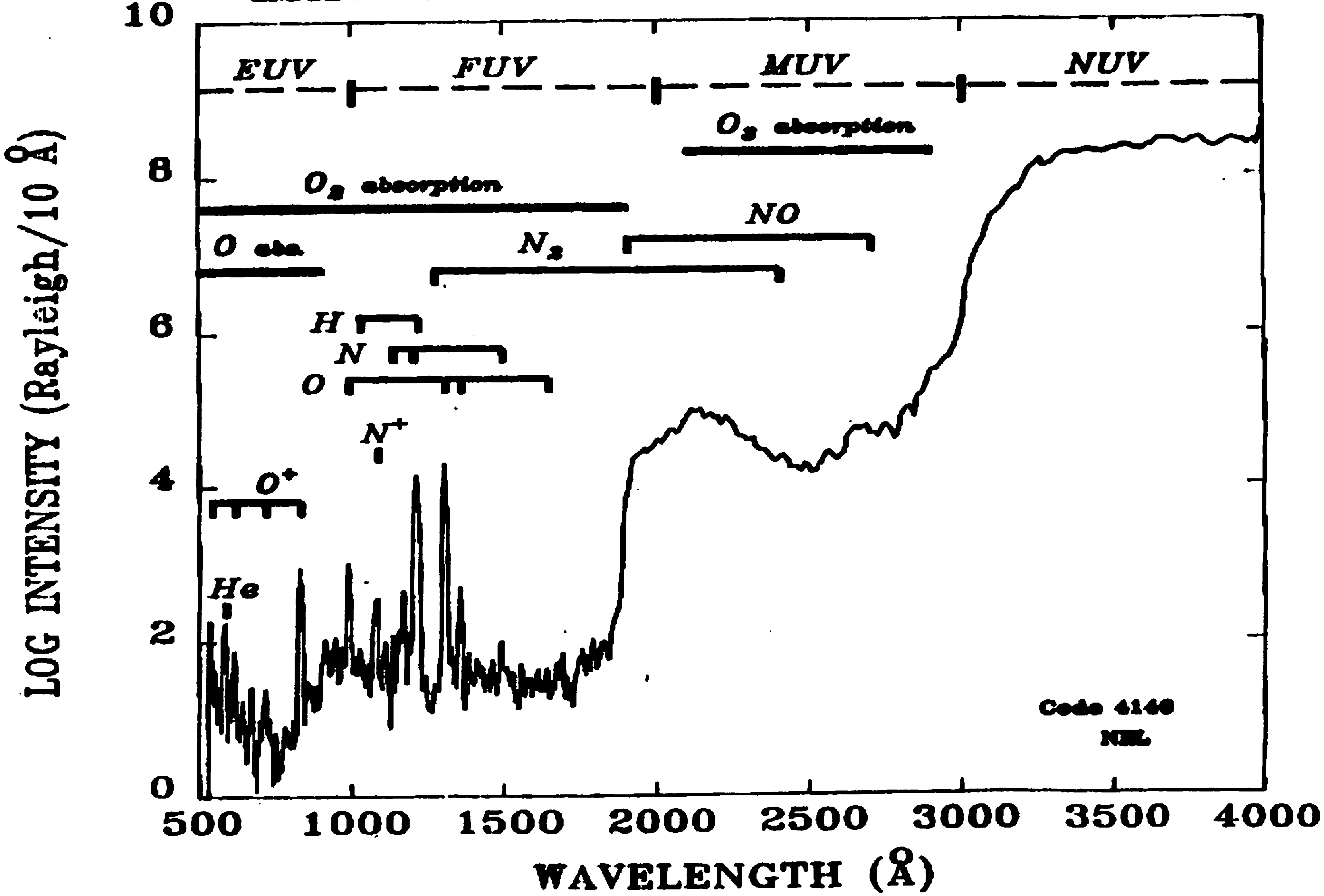

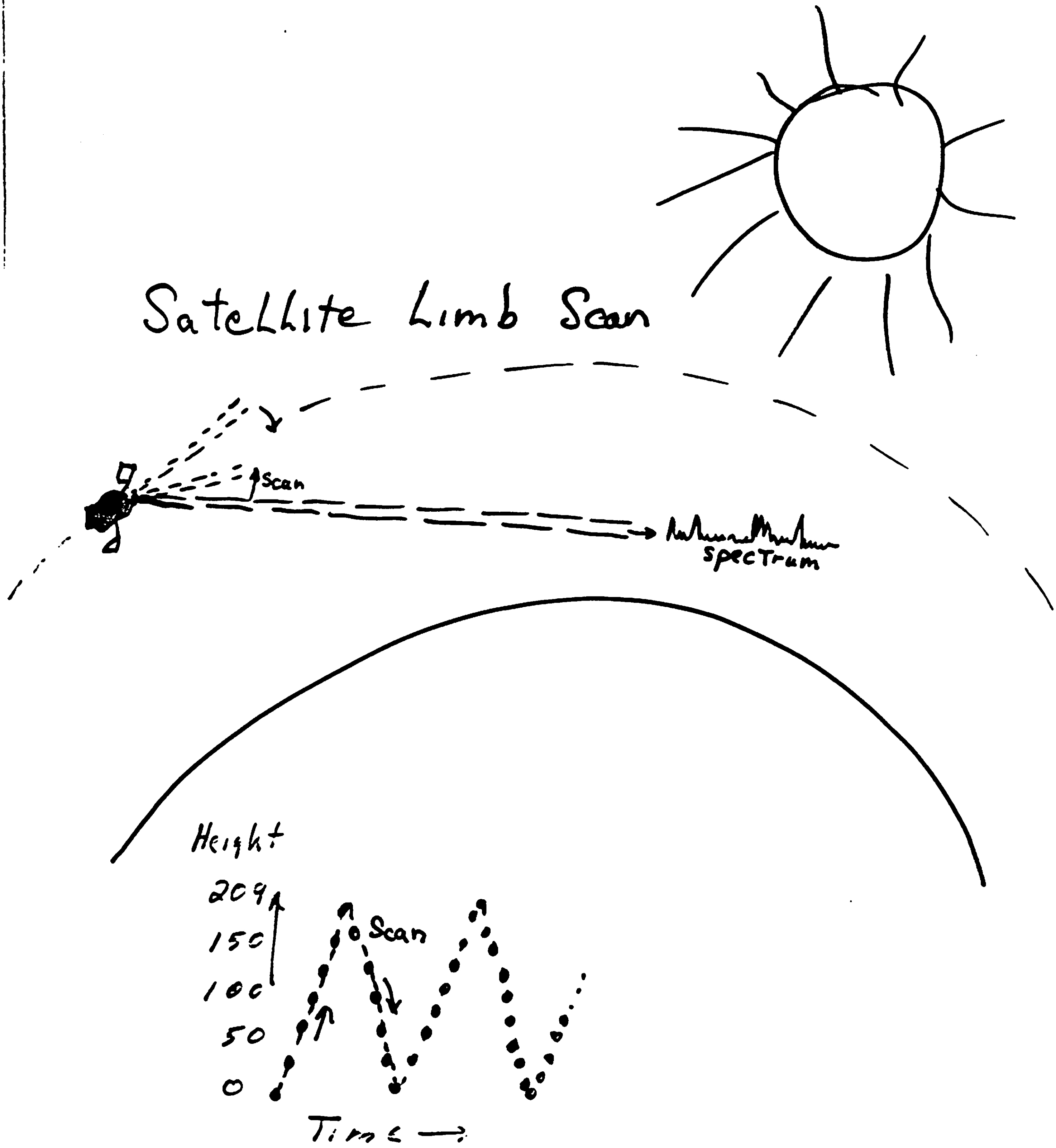
Satellite Limb Scan
Scan
Spectrum
Height
200
150
100
50
0
Scan
Time

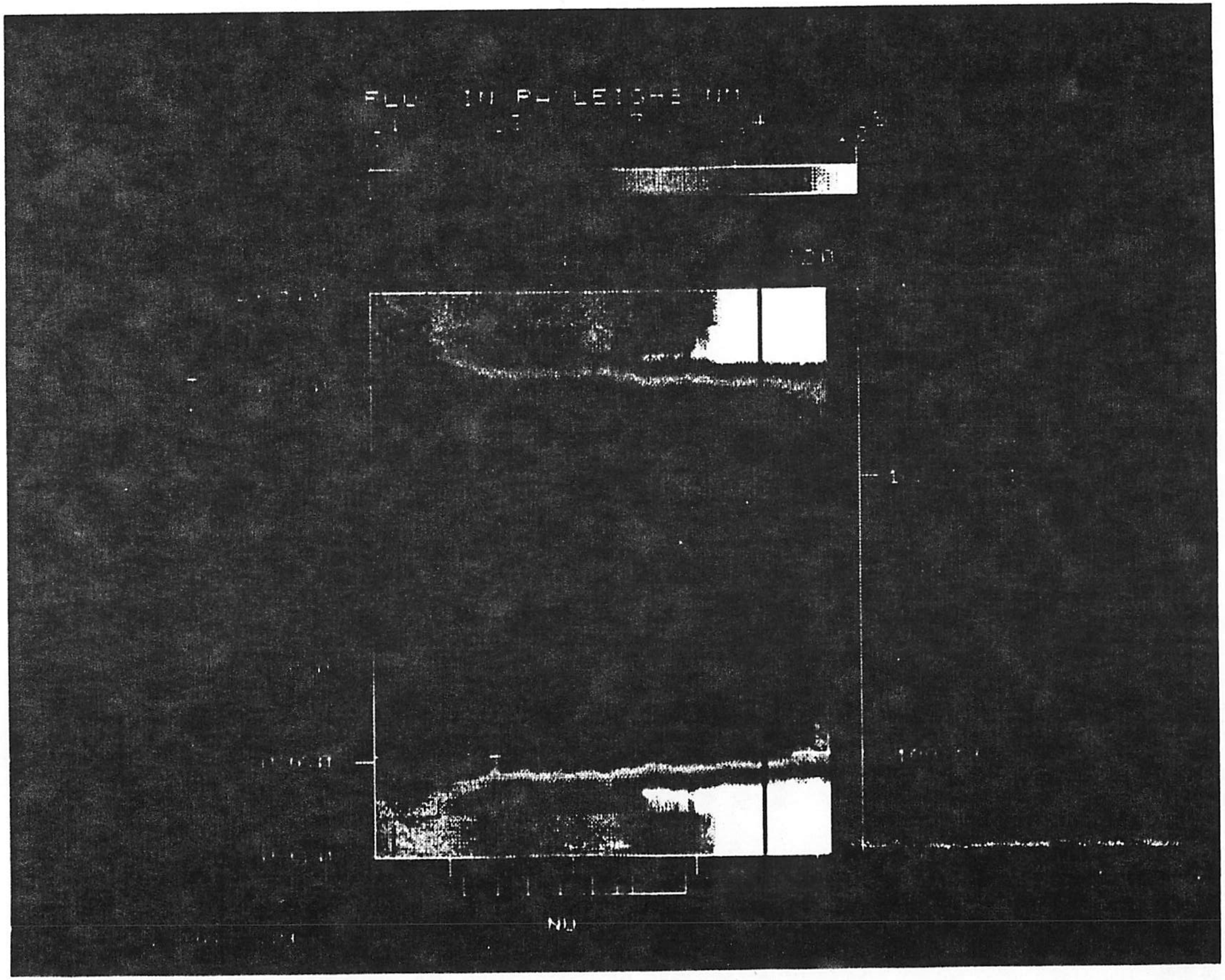
NU

(noon)

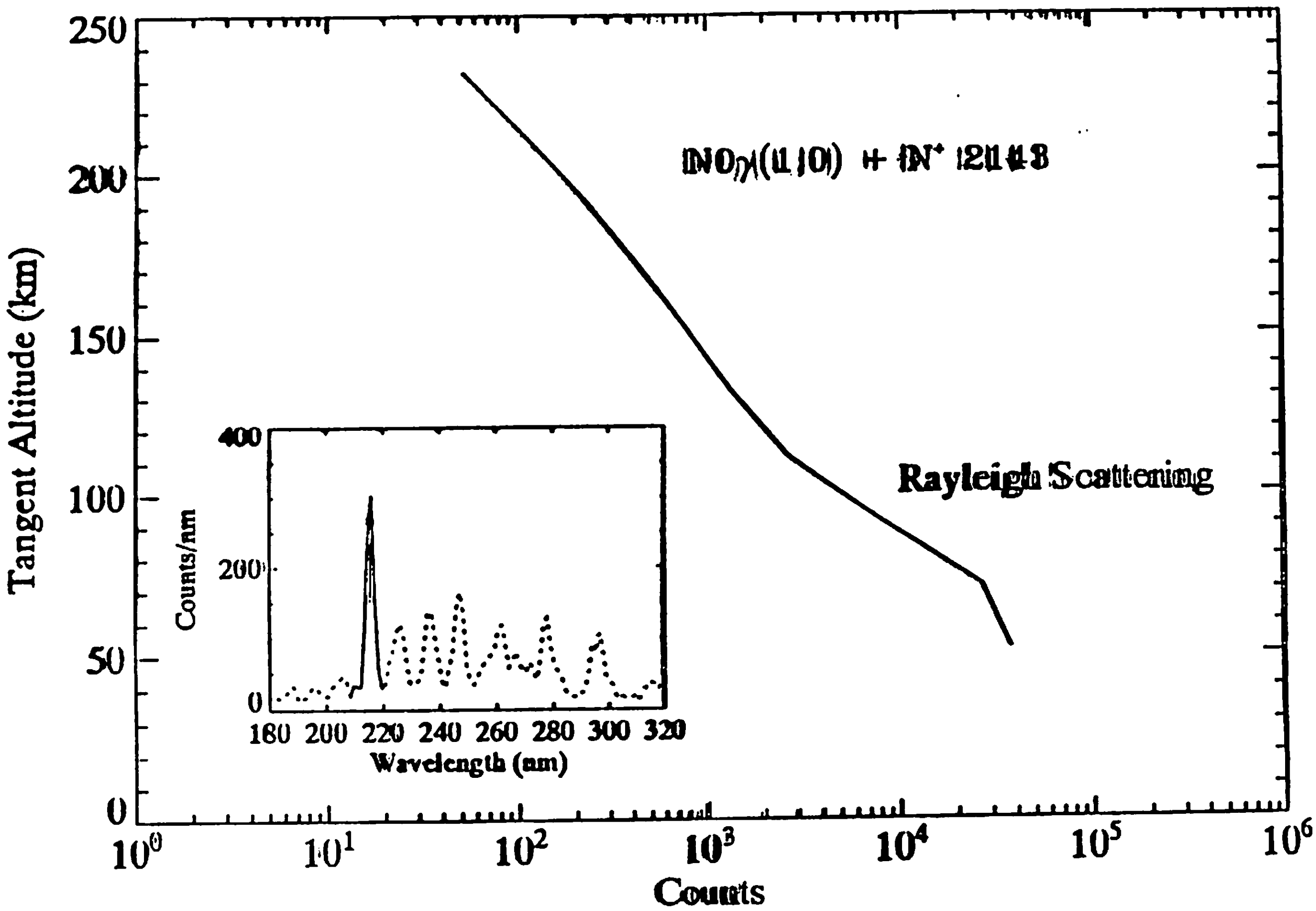

(analysis from CPI and JHU/APL

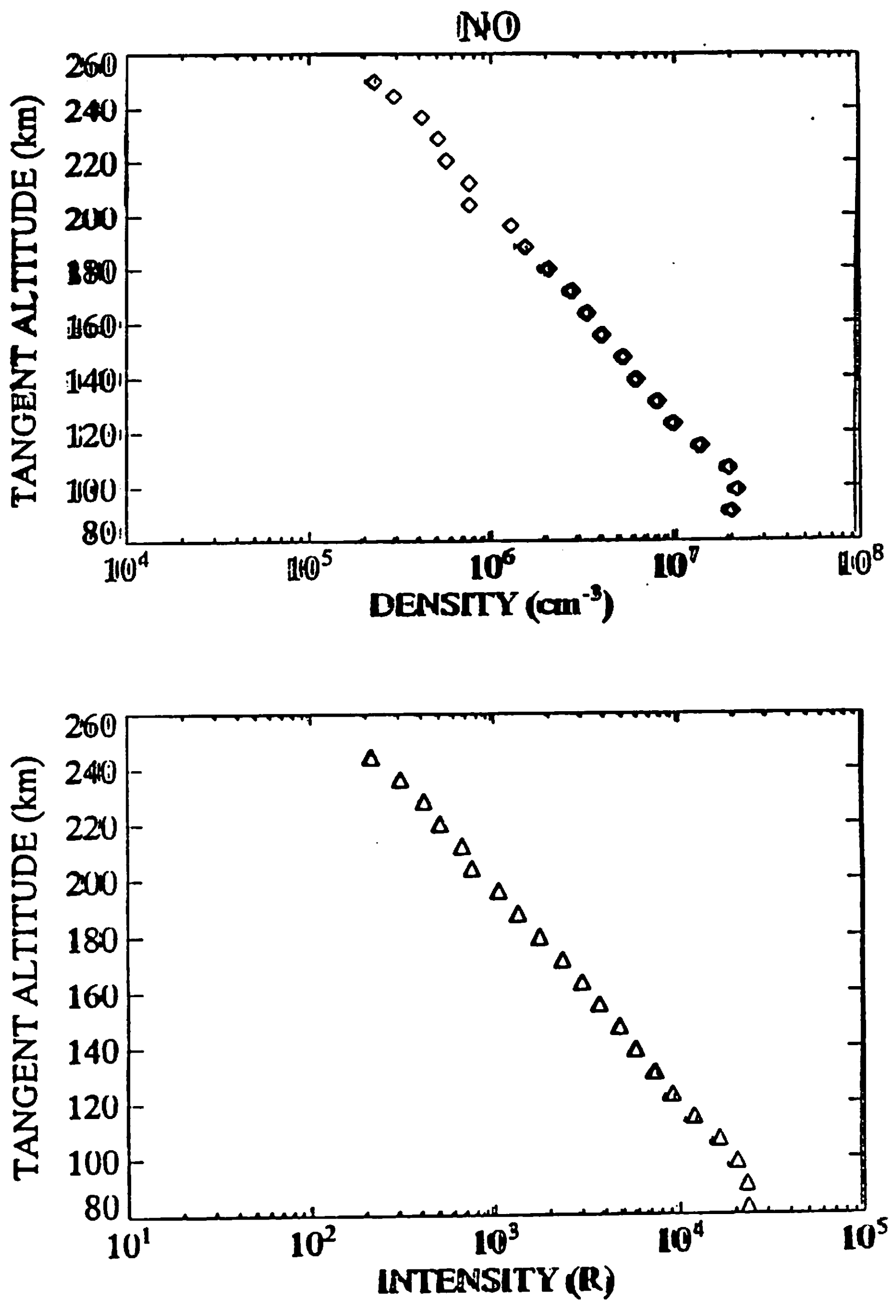

Figure 17 - Conversion of a reduced earth limb dayglow observation of the NO intensity into a NO density profile.

(Analysis from CPI and JHU/APL)

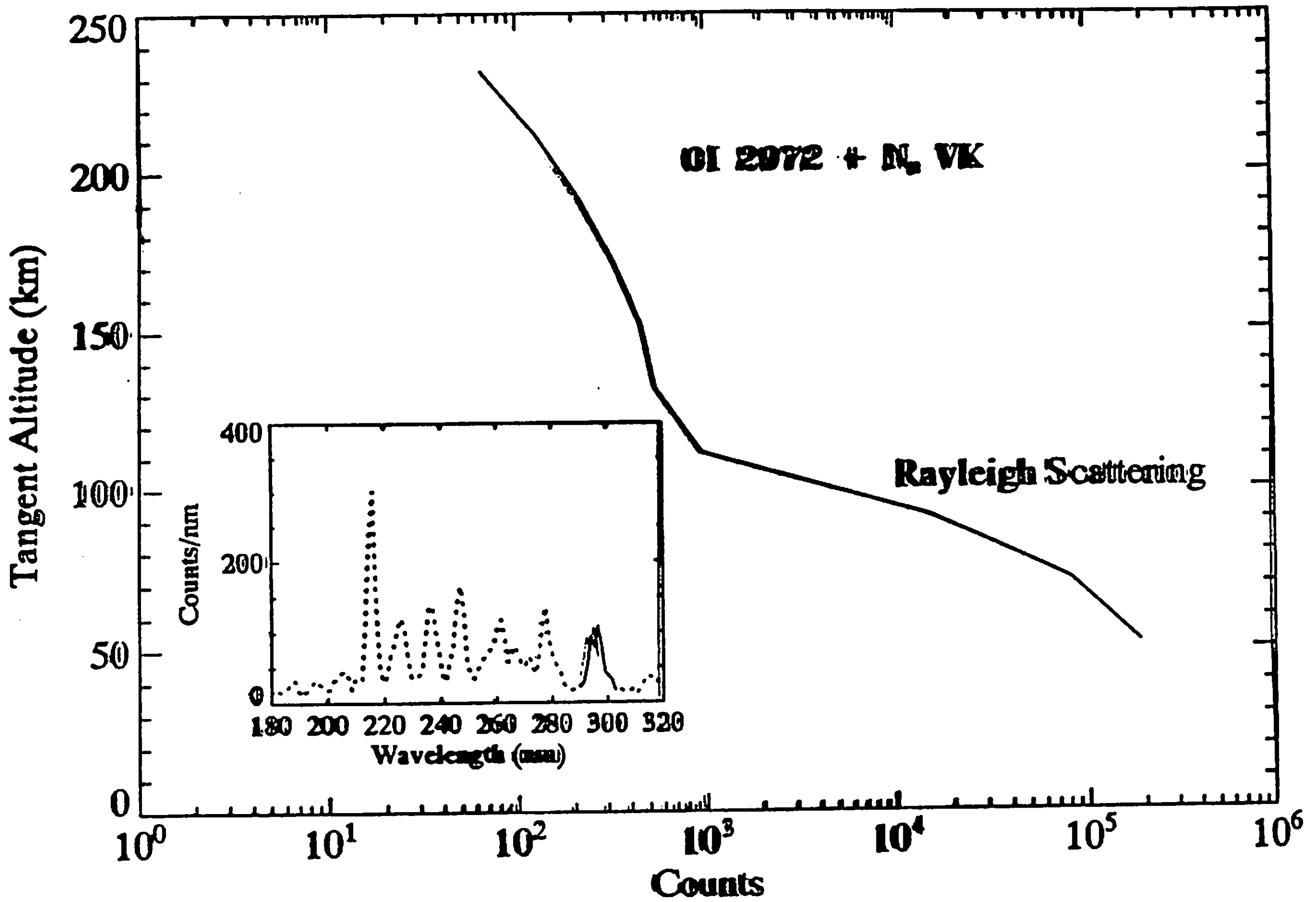

(Analysis from CPI and JHU/APL)

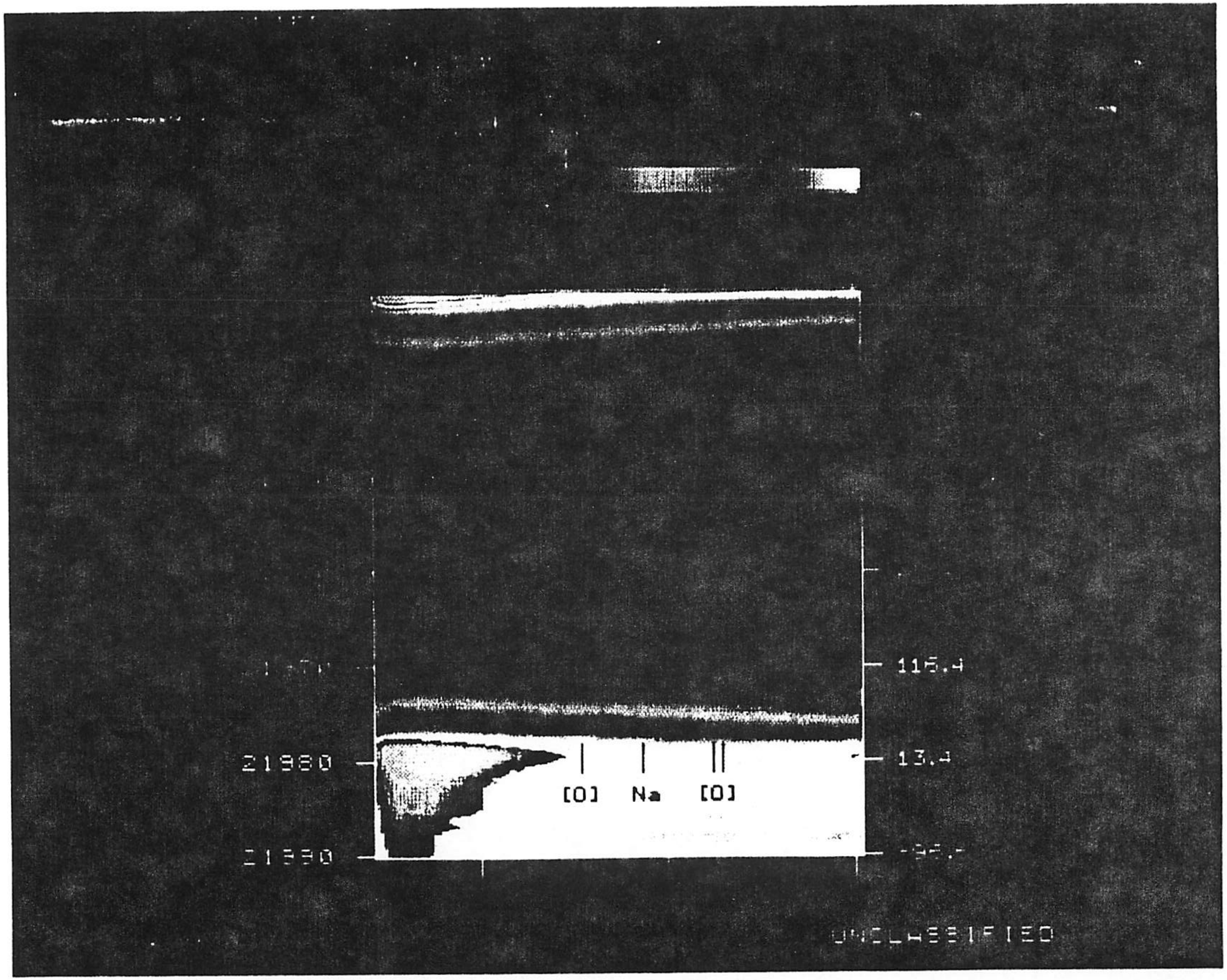
116.4
21980
13.4
[O]
Na
[O]
UNCLASSIFIED

SUMMARY

The MUV dayglow observed from a low earth orbiting satellite at 2.8 nm resolution have been analyzed. Theoretical radiances were calculated utilizing a dayglow energy deposition and radiance model. Comparison of theory and data below a tangent altitude of 80 km shows that the emission is dominated by Rayleigh scattering. As the tangent altitude rises spectral signatures of NO , N_2 , O^+ and O appear. Analysis of these emissions shows that the observed emission is consistent with currently accepted ion-neutral chemistry in the mesosphere and lower thermosphere.

The NO density deduced compares well with SME results and shows an apparent scan-to-scan variation which implies very short time scale variations in the radiation field and/or NO density. The theory consistently overestimates the data near 205 nm where both NO and N_2 LBH emit radiation. The good fit to the remaining N_2 LBH data provides a measure of magnitude of the solar EUV energy deposited in the thermosphere. The deduced NO density above 110 km is used as input to the ion-neutral chemistry model which calculates the $O(^1S)$ and $O(^1D)$ excitation rates. The neutral density background atmosphere was calculated with MSIS86 for the solar and geomagnetic conditions appropriate to the measurements. No scaling of the MSIS86 densities were required.

(Analysis from CPI and JHU/APL)

General Guidelines

1) OPTICAL Observations provide a method for remotely determining atmospheric parameters

2.) The Accuracy of these determinations depends on our knowledge of specific excitation and loss mechanisms cross sections and perhaps neutral and ion dynamics.

3.) Characteristics of the geometry of the measurement impact the resolution of the derived parameter.

4) Simultaneous observations of different emissions are necessary to evaluate models which link emissions to atmospheric parameters.

Coordination with Rockets

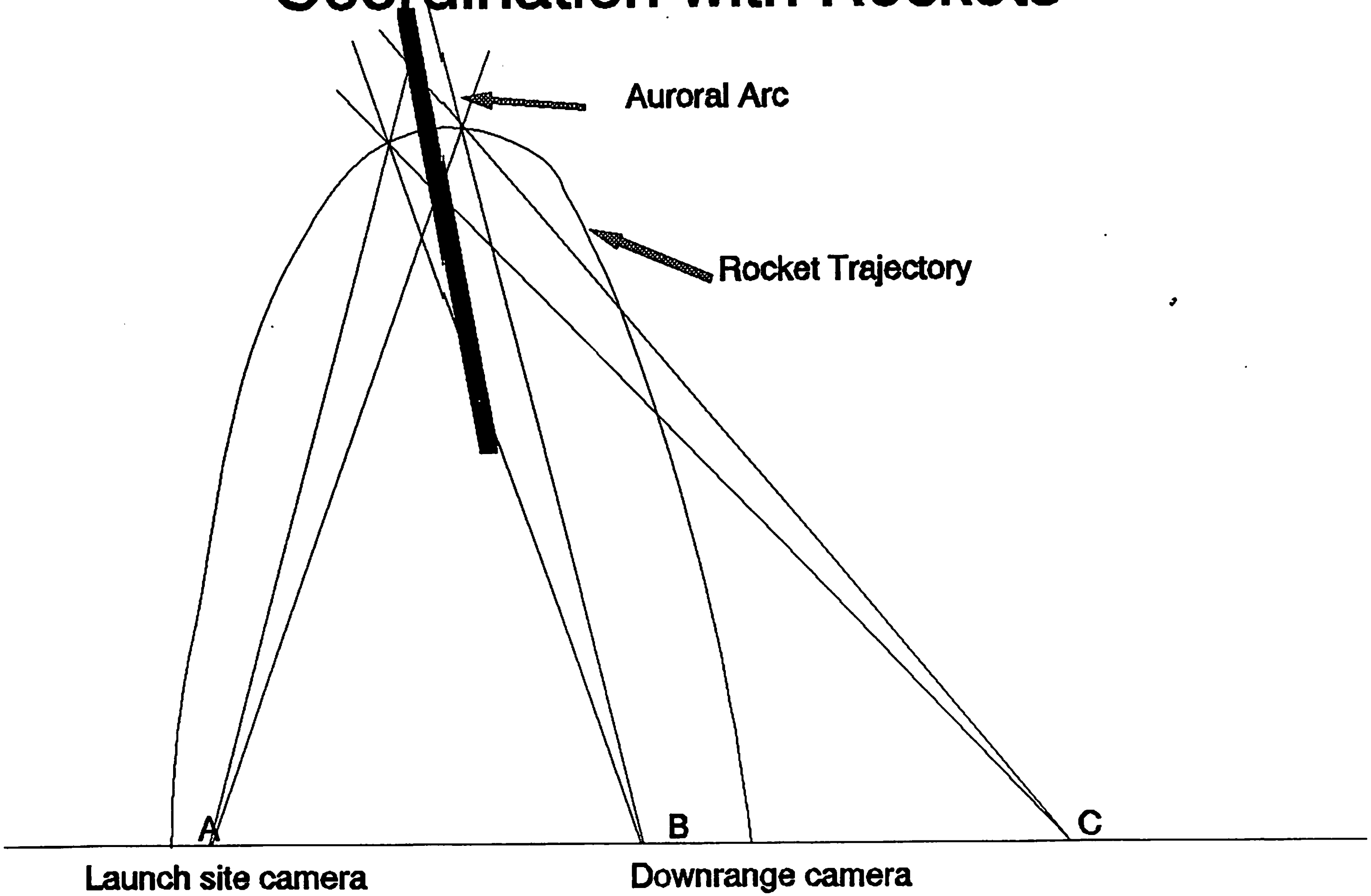

Tomographic Meridian Scanning Photometer Group at A, B and C

Coordinated Experiments with Incoherent Scatter Radars

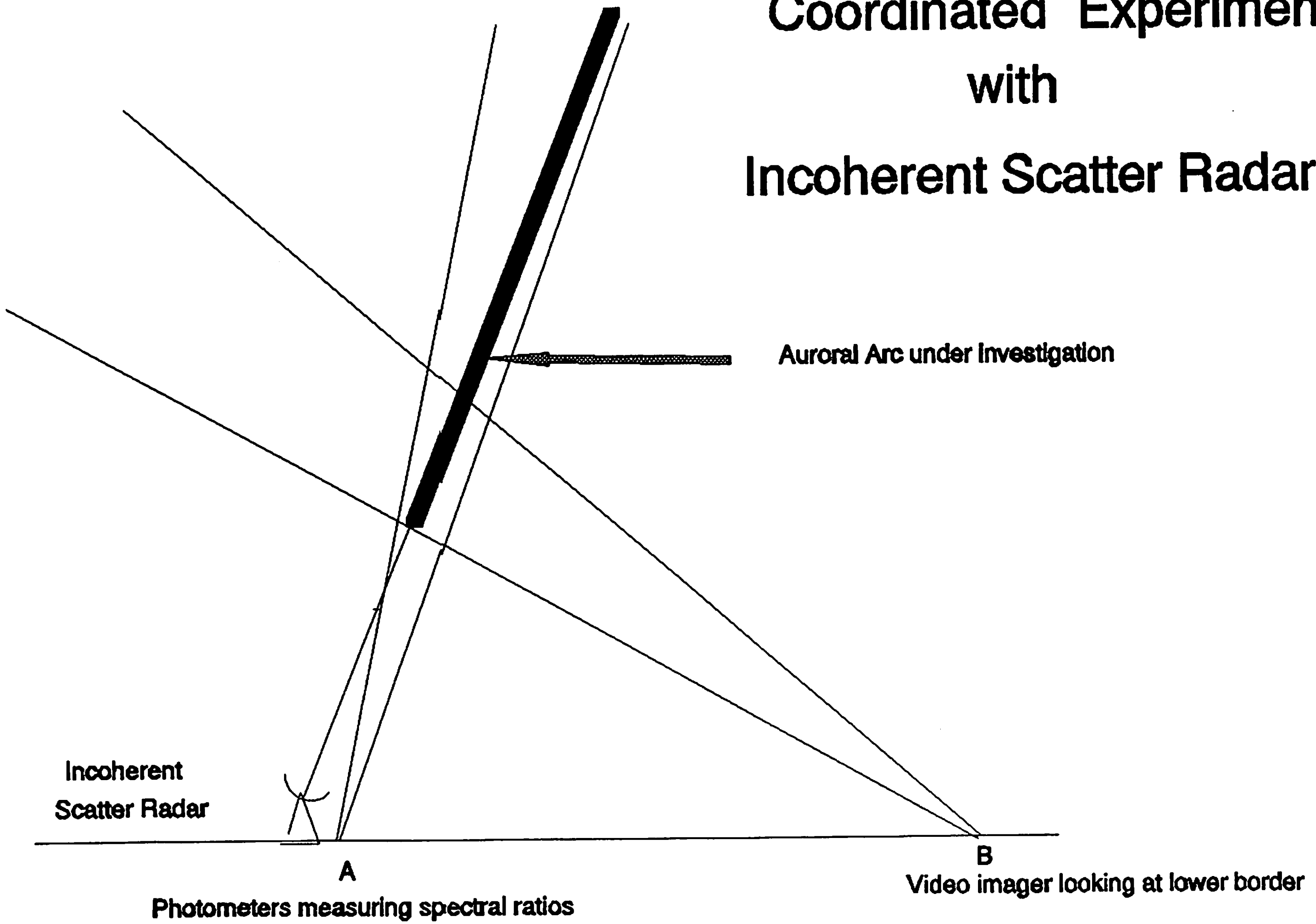

THE PHOTOMETRIC MATRIX

$I_\lambda(x,y,t)$

* Imaging data fills in the values in this 3-D matrix. The instrument is truly multiplex, ie all dimensions in the matrix are filled at once.

* Data studies are usually shown in 2-D extracts. For any given position in the imaged field, "post-hoc" photometry can be performed giving

$$I_{x,y,\lambda}(t).$$

* Alternatively we can study spatial variations at an instant:

$$I_{\lambda,t}(x) \text{ or } I_{\lambda,t}(y)$$

* Studies in any of these spatial or temporal series must be done in the awareness that layer height and geometry can change without any direct knowledge from the measurement.

* Calibrations in intensity, flatfielding, optical distortion, and photometric linearity are required before that data have a scientific value. Also error bars must be determined.

Photometric Imager

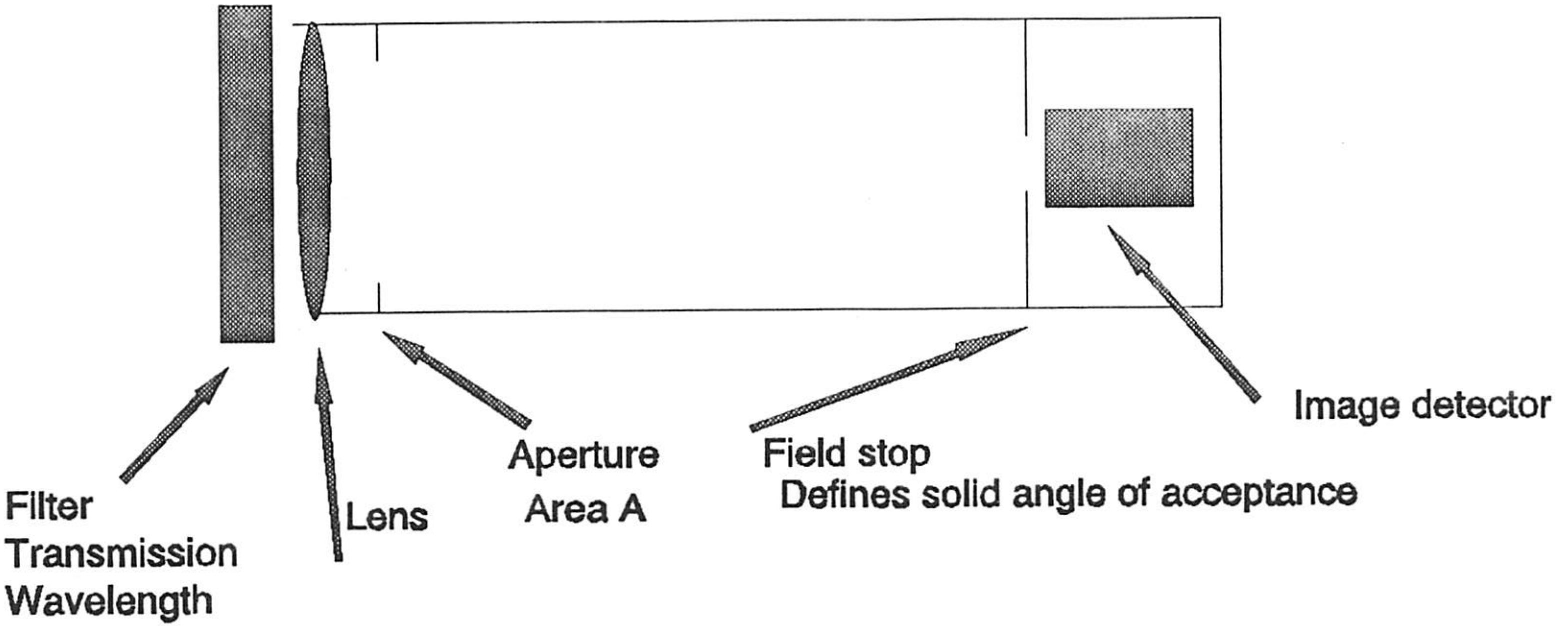

$$I=\frac{A\Omega}{4\pi}X10^{6}\tau_L\tau_F Q$$

A = the aperture of the optical component
Ω = the solid angle of acceptance of the component
τ_F= the transmission of a prefilter
τ_L= the transmission of the lens or other component
Q = the quantum efficiency of the detector

Flying Spot Imager

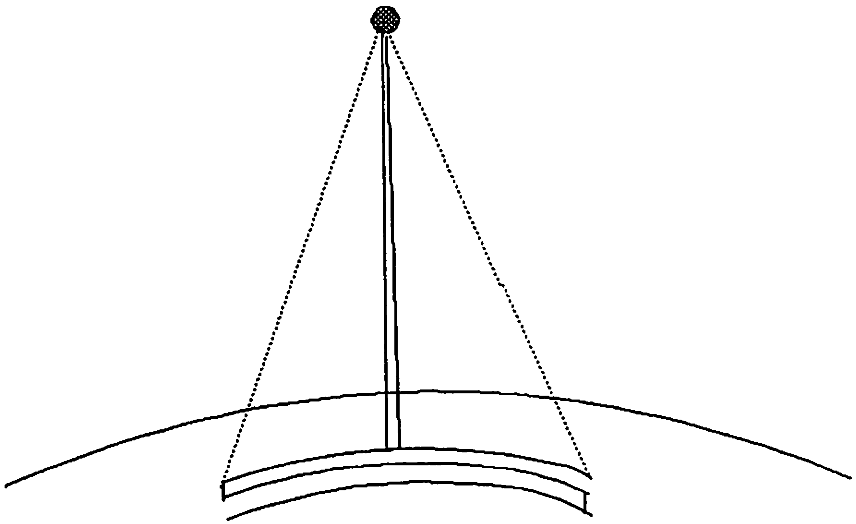

Light received from zig-zag track

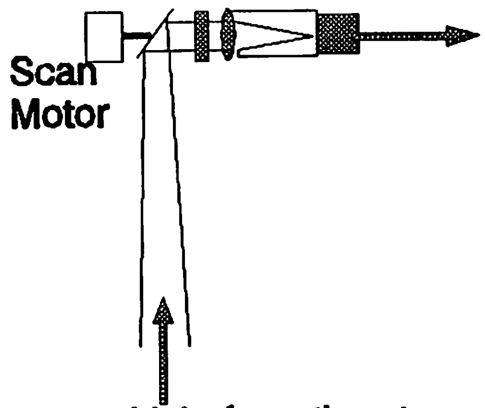

Data quality depends upon the sensitivity and noise performance of the single channel photometer, and the brightness of the light source in the atmosphere.

The Imaging Photon Detector

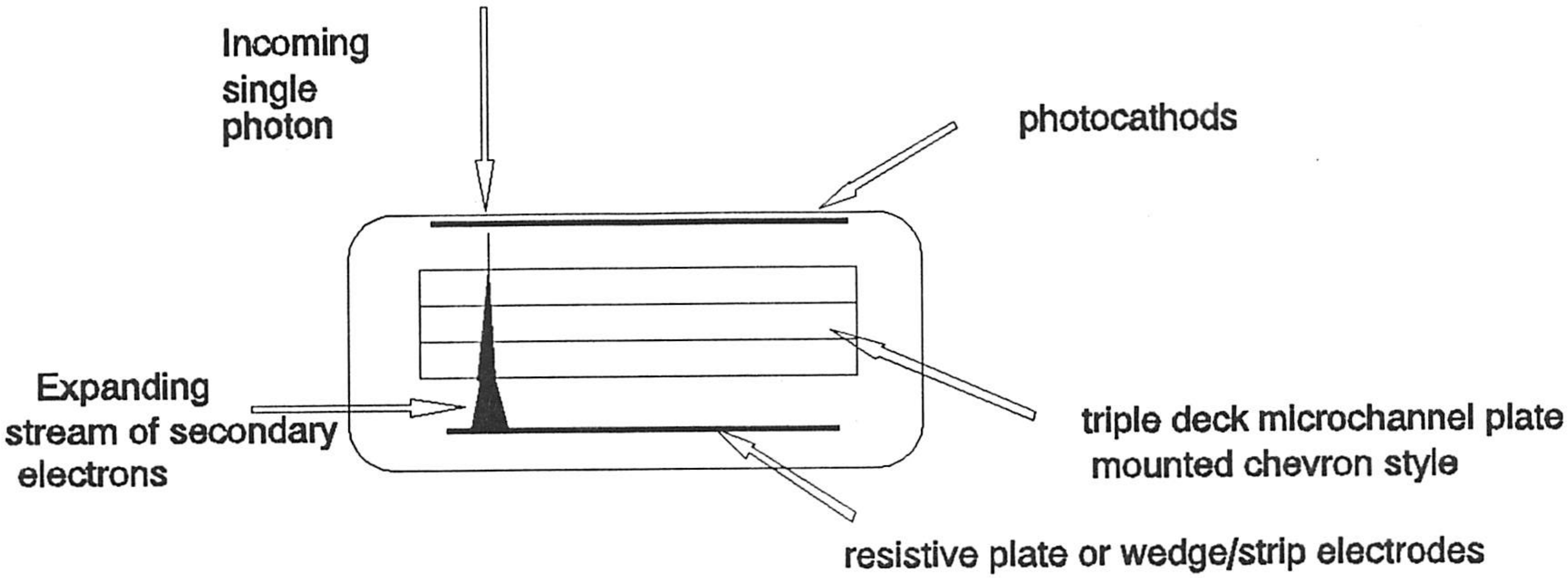

$$x = \frac{(A+B) - (C+D)}{A+B+C+D}$$

$$y = \frac{(B+C) - (A+D)}{A+B+C+D}$$

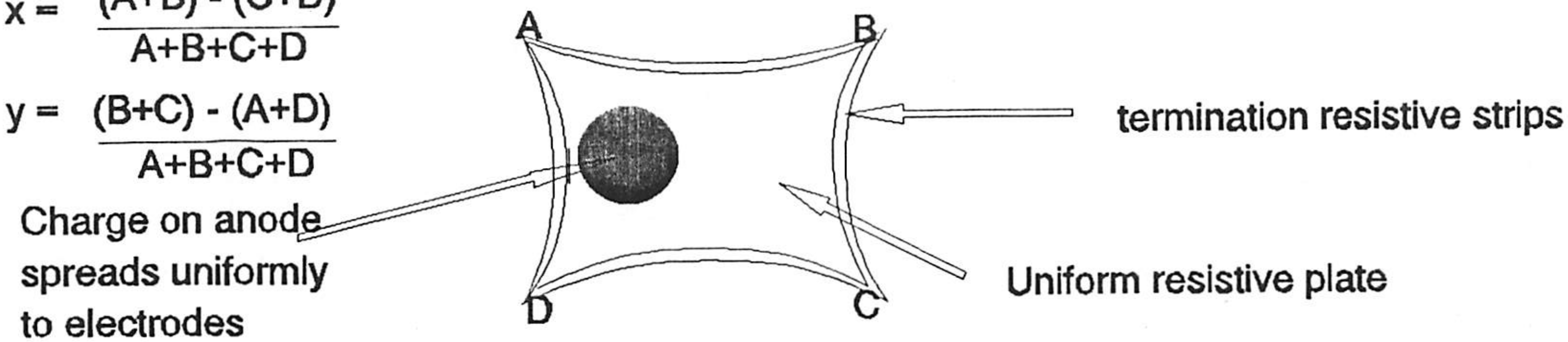

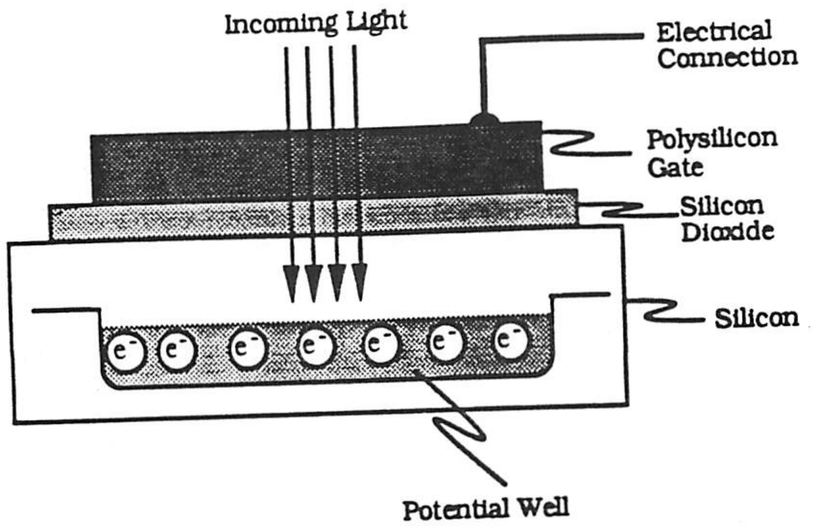

Figure 2-2. Cross-Section of a Simple Photodetector

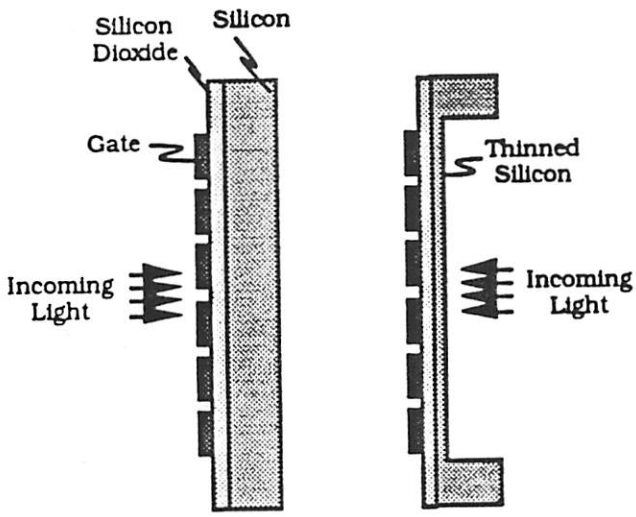

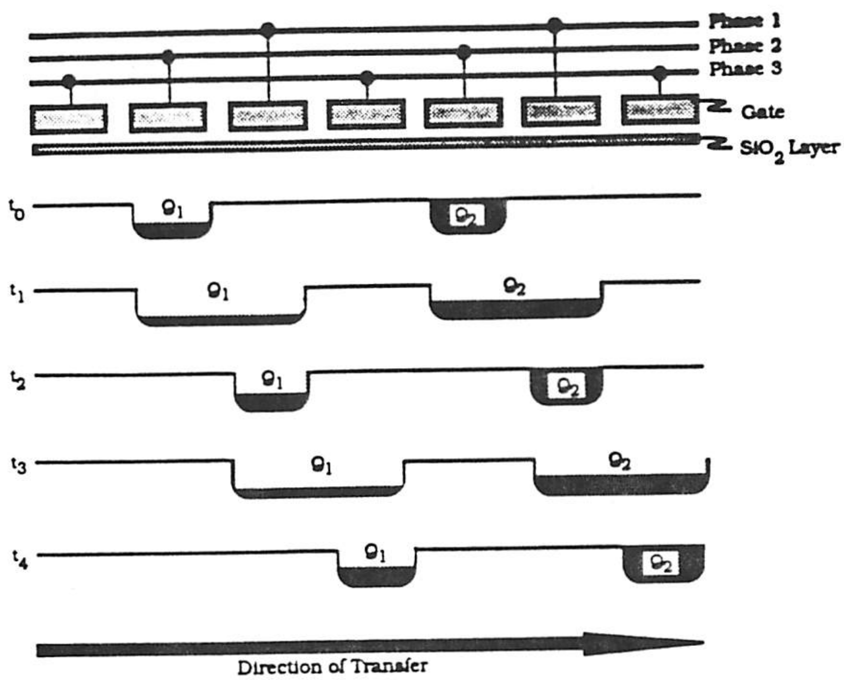

Figure 2-3. Charge Transfer in a 3-Phase CCD

Image Intensifiers

Devices which convert an optical image to electronic form, amplify the signal and convert back to optical.

Conversion to electronic form is by a photocathode.
Amplification may involve secondary electrons
Conversion back to an optical image is by phosphor.

Focussing can be magnetic or electrostatic. (proximity).
Here is an electrostatic type.

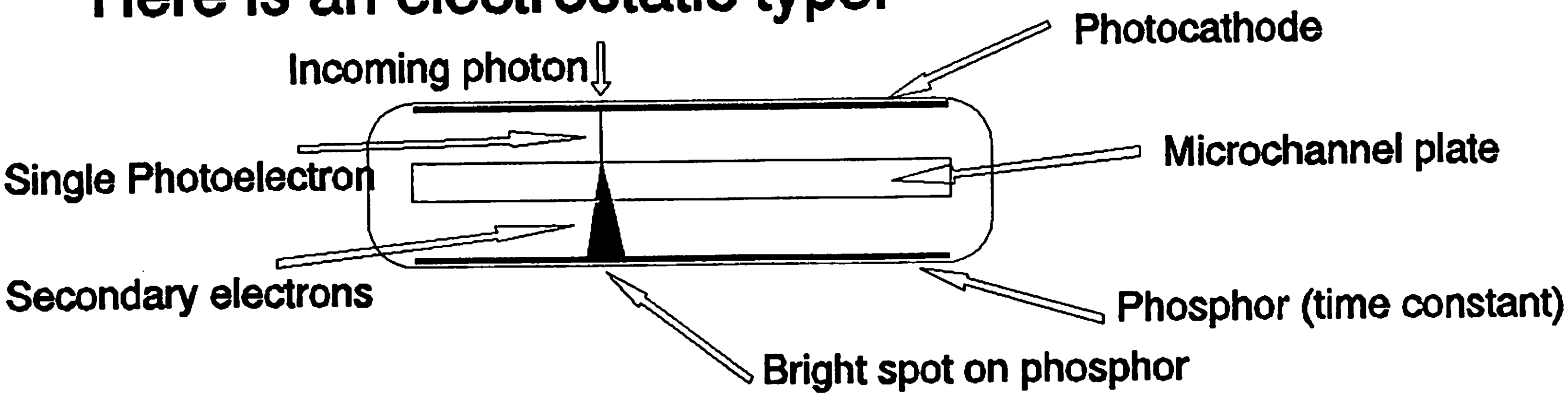

TABLE OF COMPARISON

Criterion	CCD	IPD	Flying Spot
Wavelength sensitivity	<4000Å – 11000Å	S25 3000–7500Å GaAs <4000–9000Å	>25 GaAs Bi-Alk UV.
Read noise	2–10e/pix at 50MHz (increases with A/D speed)	N/A	N/A
Thermal noise	0.5e/s at −50°C using MPP* bias	1.5×10^{-3} e/s at 0°C for S25	1–2 s^{-1} dependent on cooling and photocathode
Spatial non-linearity	<0.2%	~1%	depends on satellite stability and scanning mirror ~0.1%.
Photometric non-linearity	V. small up to full well.	dependent on dead time in processing and on any mcp** overload.	linear over 3-4 OM
Image brightness limitation	Full well ~250k electrons	mcp** overload dependent no limit on pixel storage except in computer.	dead time limited

* Multi-pinned phase

** microchannel plate.

Effect of diffraction on the image of a point source

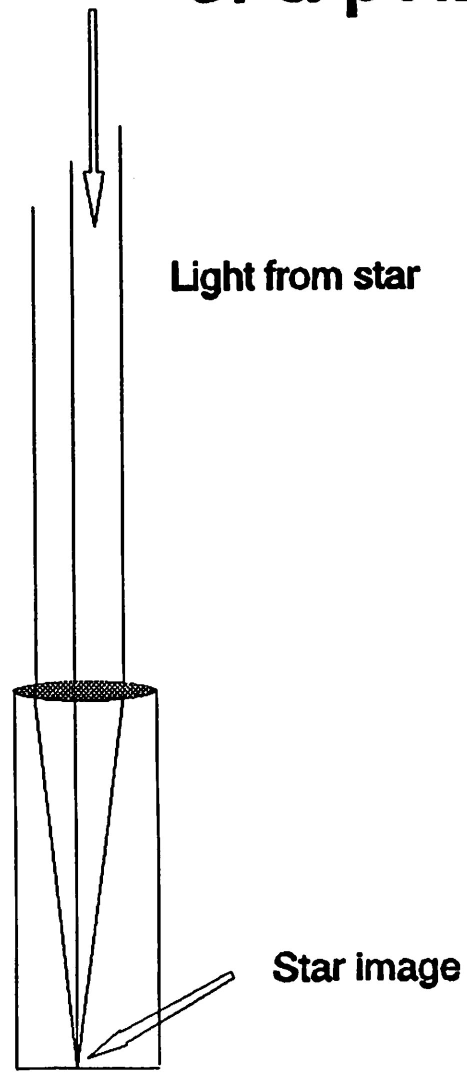

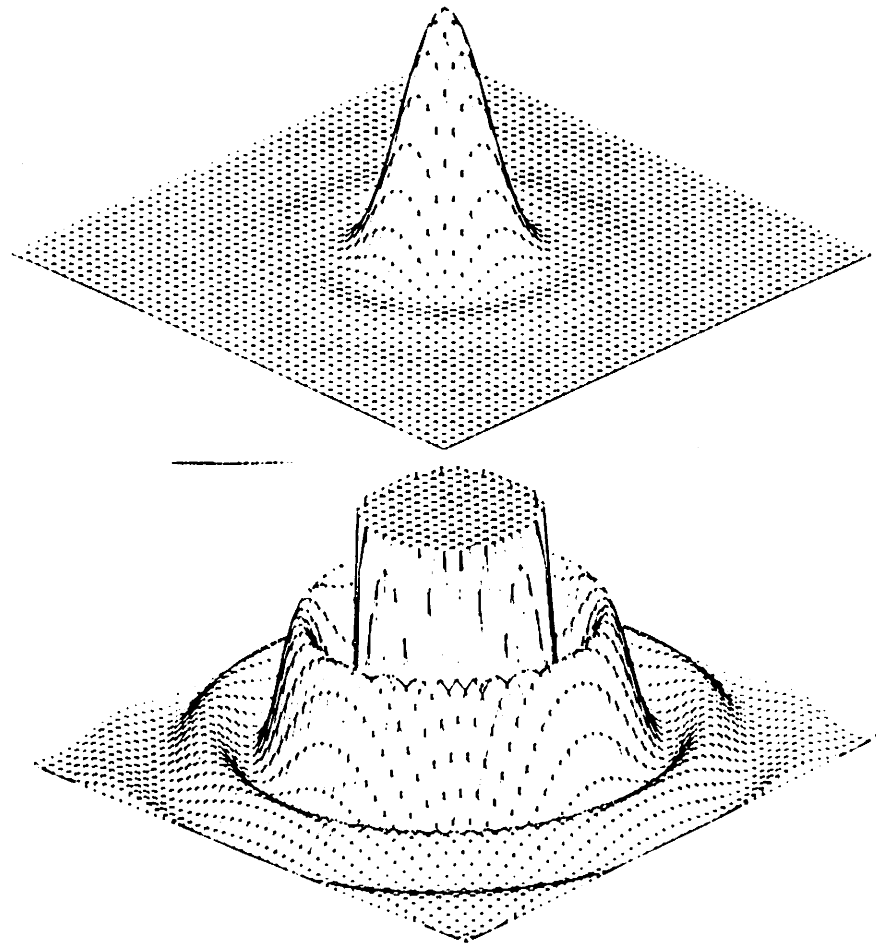

Vignetting

Some off-axis rays are obstructed by camera structure

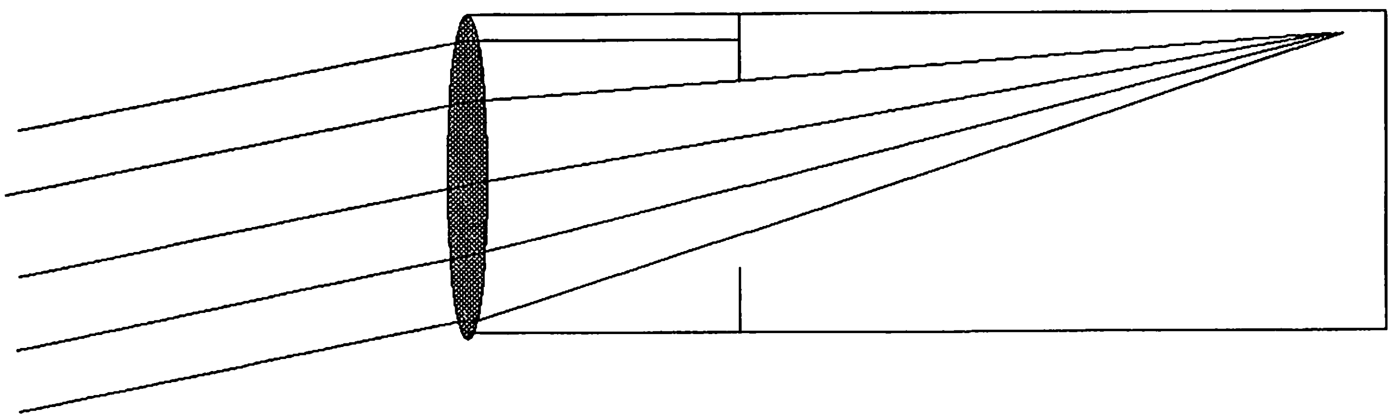

Aberrations

Spherical

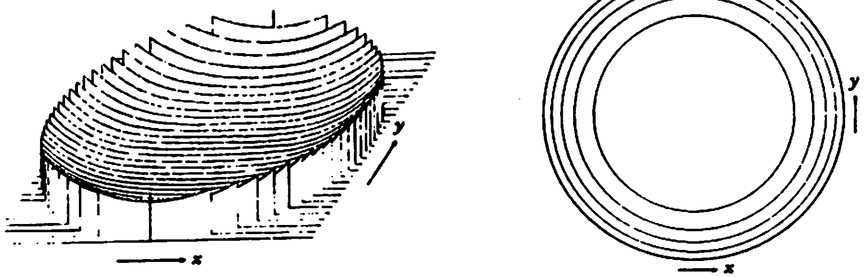

Astigmatism

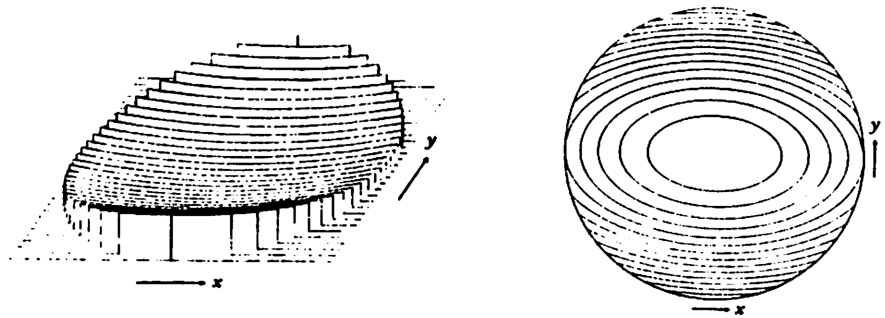

Coma

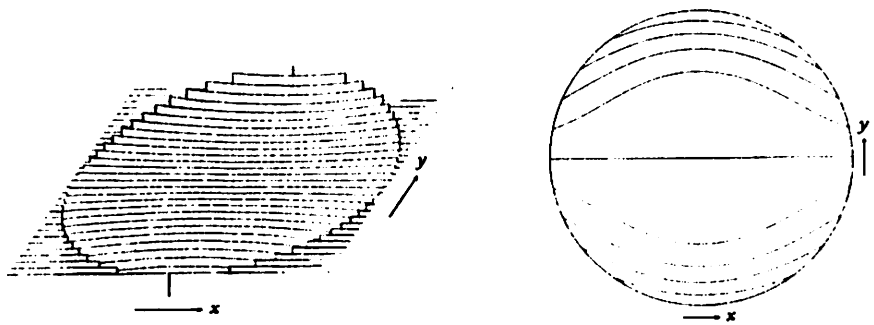

CONSTANCY OF AΩ

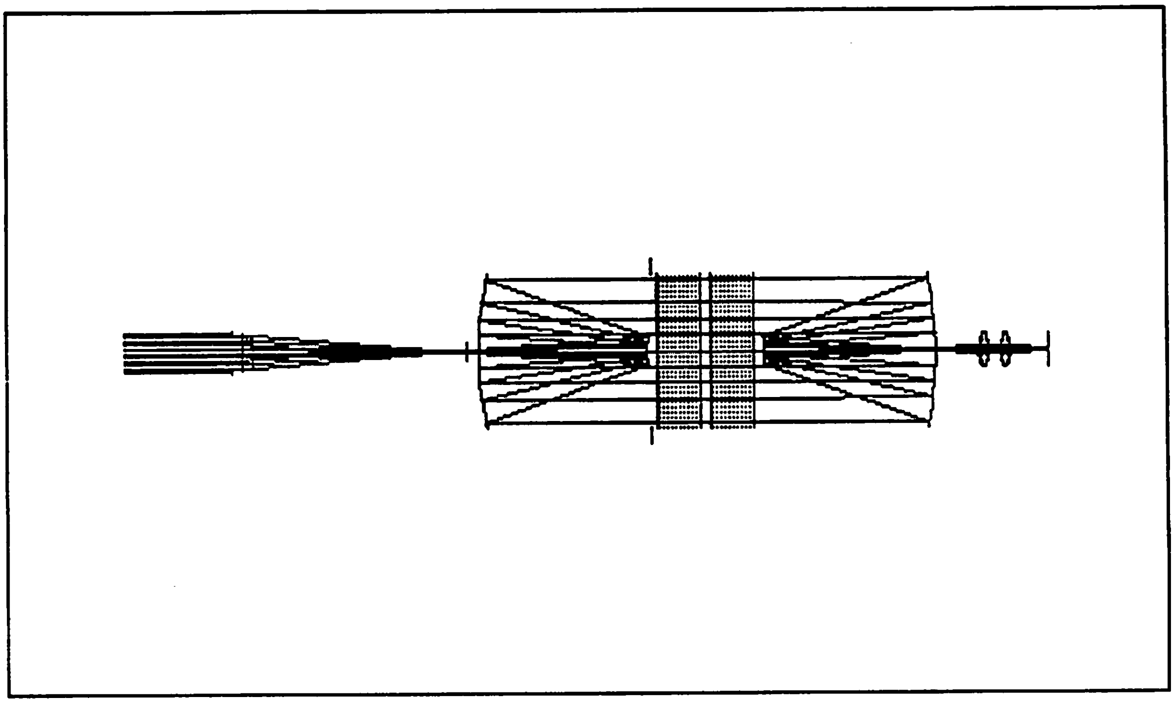

$$I = \frac{A\Omega}{4\pi} X 10^6 \tau_L \tau_F Q$$

A = the aperture of the optical component
Ω = the solid angle of acceptance of the component
τ_F= the transmission of a prefilter
τ_L= the transmission of the lens or other component
Q = the quantum efficiency of the detector

Data Storage

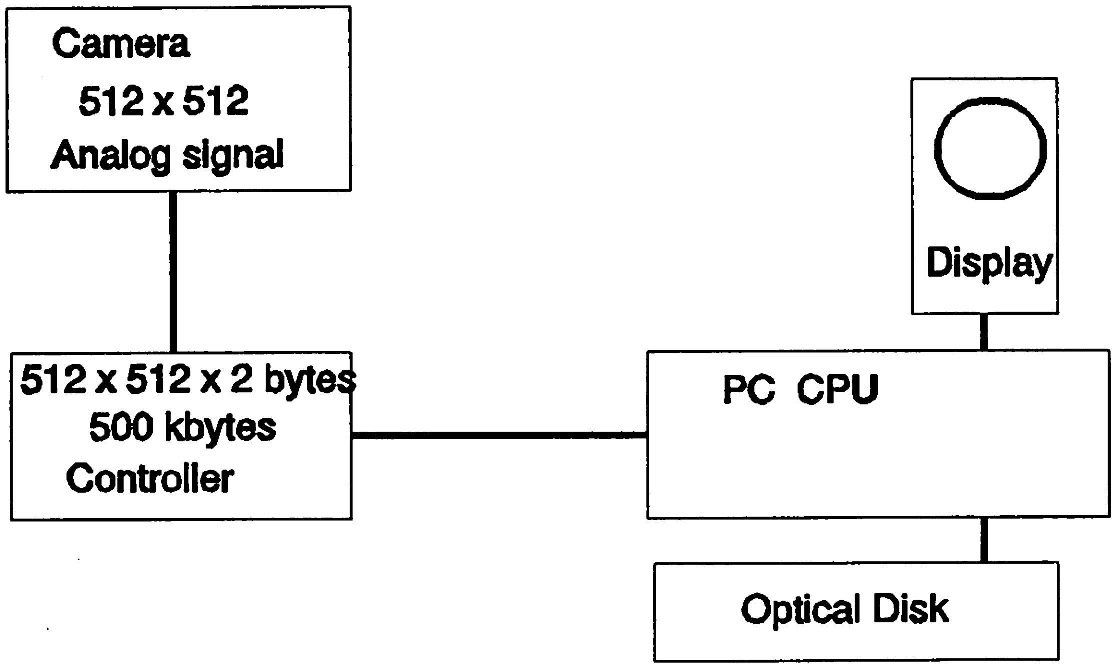

Imaging Speed

- Depends on shot, dark and read noise.
- Limited by speed of data handling and transfer to disk.
- For IPD also limited by the serial processing time.

THE SPECTROPHOTOMETRIC MATRIX

$I(\lambda,x,t)$

* Data matrix in 3 dimensions:
  1 spectral, 1 spatial (along the slit), 1 time.

* Data studies (often 2-dimensional):

  - Spectral type:
    Spatial variations $I_t(\lambda,x)$
    Temporal variations $I_x(\lambda,t)$

  - Photometric study of one feature:
    Spatial variations $I_\lambda(x,t)$
    Temporal variations $I_\lambda(t,x)$

* Geometrical factors, such as the van Rhijn effect need to be considered in any spatial studies.

Spectral Information in lines and bands

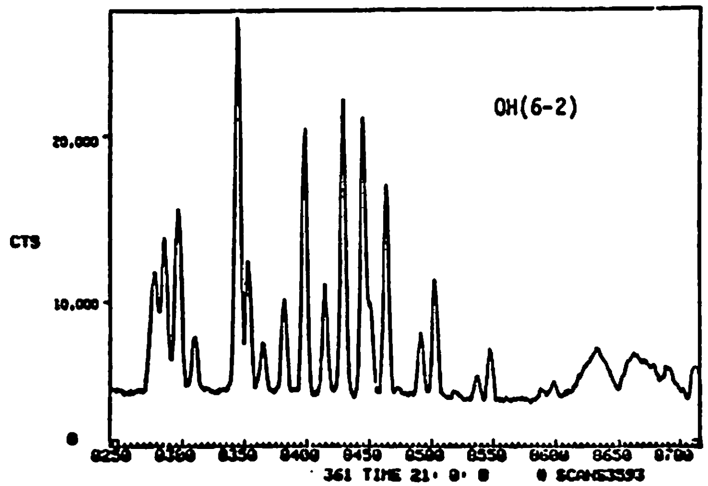

Line and band intensities

Most information can be obtained with between 1 and 5A resolution.

Peak shift
47.6 m/s /mA at 6300A

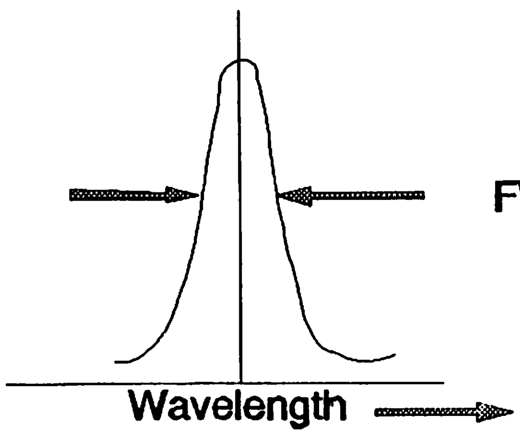

Spectral line shapes

FWHH = k x SQRT(T/M)
= 23.3 mA for 5577A OI at 200K
= 59.4 mA for 6300A OI at 1000K

GENERALIZED SPECTROMETER

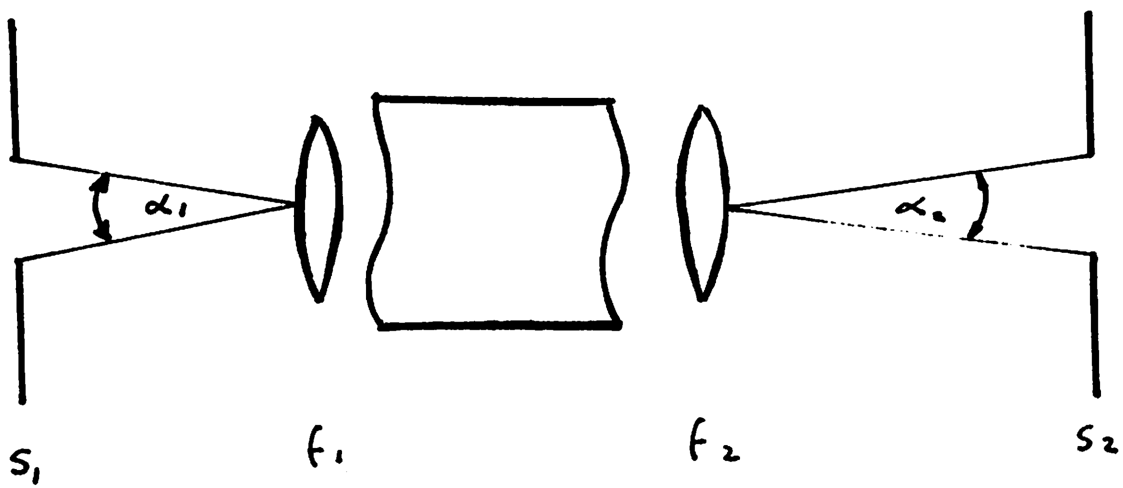

Spectral Properties:

a) Color (Wavelength).
b) Shape.
c) Area.
d) Time behavior.

Wavelength:

λ, expressed at 1 atmosphere, 15 C. $\sigma = \lambda_o^{-1}$, expressed in wavenumbers (cm^{-1} . λ_o: vacuum wavelength.

Resolving limit:

$\delta\lambda$: smallest resolvable spectral element, in wavelength. $\delta\sigma$: smallest resolvable spectral element, in wavenumbers.

Resolving power:

$$R = \delta\lambda \;/\; \lambda = \delta\sigma \;/\; \sigma \;.$$

Flux delivered to the detector:

$$F = I \; A \; \Omega \; \tau \;.$$

Luminosity:

$$L = F \;/\; I = A \; \Omega \; \tau \;.$$

Angular dispersion:

$$D = d\beta / d\lambda = d\beta / d\sigma \;.$$

Spectral width:

$$\omega = \Theta \;/\; D \;.$$

A spectrometer has a slit (or aperture) with angular width Θ and angular height Φ. The transmission properties for this aperture are given by $\tau(\Theta, \Phi)$. The associated solid angle is:

$$\Omega = \int_0^{2\pi} \int_0^{\Theta/2} \tau(\Theta, \Phi) \sin\Theta \, d\Theta \, d\Phi \, .$$

$$\Omega = 2\pi \left[1 - \cos(\Theta/2) \right] \simeq \Theta^2 \qquad \text{(circular aperture)} \, .$$

$$\Omega \simeq \Theta\Phi \qquad \text{(otherwise)} \, .$$

$$L \simeq A \, \tau \, \Theta \, \Phi \quad \text{or} \quad A \, \tau \, \Theta^2 \, .$$

For one-dimensional dispersion devices, such as a grating or prism spectrometer:

$$\Theta = \omega \, D \, .$$

$$L_{sp} \simeq A \, \tau \, \Phi \, \omega \, D = A \, \tau \, \Phi \, D \, \lambda \, R^{-1} \, .$$

For two-dimensional dispersion devices, such as Michelson and Fabry-Perot spectrometers:

$$\omega = \sigma \, \Theta^2 \, 8^{-1} \, ,$$

$$L_{FP} \simeq A \, \tau \, 8 \, \omega \sigma^{-1} = A \, \tau \, 8 \, R^{-1} \, .$$

For the specific case of a grating spectrometer at near-normal incidence with a grating with a blaze angle γ:

$$D = N \, n \, (\cos\beta)^{-1} \quad ; \quad \sin\alpha + \sin\beta = N \, n \, \lambda \, ,$$

$$D = A \, (\sin\alpha + \sin\beta) \, (A \cos\beta \, \lambda)^{-1} .$$

$A\ \cos\beta = A_o$, where A_o is the area normal to the beam. In addition, $\sin\alpha + \sin\beta = \sin(2\gamma)$.

$$A_o\ D = A\ \sin 2\gamma\ \lambda^{-1}\ ,$$

$$L_g = \tau\ \Phi\ A\ \sin 2\gamma\ R^{-1}\ .$$

The comparison of the luminosity between these two types of dispersing spectrometers, **at equal resolving power**, assuming equal area grating and interference spectrometer pupils, is:

$$[\ L_{FP}\ (\ L_g\ )^{-1}\ ]_{A_{FP} = A_g} = 8\ (\ \Phi\ \sin 2\gamma\ )^{-1}\ .$$

For a typical grating with a blaze angle near 15° and a spectrometer with an angular height of 0.2 radians:

$$[\ L_{FP}\ (\ L_g\ )^{-1}\ ]_{A_{FP} = A_g} = 8\ (\ 0.2 \times 0.5\ )^{-1} \simeq 80\ .$$

This comparison shows that, for the same resolving power, a 0.5 inch by 0.5 inch interference filter (a special case of a Fabry-Perot device) is as luminous as a grating spectrometer with a 4 inch by 5 inch grating.

Because of the larger luminosity of the two-dimensional dispersing devices, their use is preferentially directed to high-resolution studies where spectral line shapes and width measurements are desired.

The, simple, instruments described above have a **Luminosity × Resolving-Power** product that is constant. However, there exist another class of instruments that are inherently **compensated** or can be compensated. A compensated device has the property of a **Luminosity** × **Resolving-Power** product that *increases* with increasing Resolving Power. They will not be discussed here.

Purposely, the above discussion has been limited to the flux delivered to the detector, and this detector is considered to be large enough to accept the flux for one resolvable element. A single detector requires that the spectrum be scanned across this detector, while a multiple detector device can observe many spectral elements simultaneously (multiplexing). For intrinsically-noisy detectors, it is possible to detect multiple wavelengths simultaneously and still have a net gain (Fellgett advantage). This technique is employed with Michelson devices in the infrared region.

Finally, there is the topic of selectivity, that is the ability of a given spectrometer to observe an arbitrary region of the spectrum without instrumentally-caused contamination from other regions. In general, grating instruments have greater selectivity, although interference devices can be made to approach this selectivity.

Selected References

F. A. Jenkins and H. E. White, *Fundamentals of Optics*, McGraw-Hill, Inc., New York, 1976

R. W. Wood, *Physical Optics*, Optical Society of America, Washington, 1988

G. Hernandez, *Fabry-Perot Interferometers*, Cambridge University Press, Cambridge, 1988

Born, M. and E. Wolf. *Principles of Optics*, The MacMillan Co, New York, 1954

OVERLAPPING ORDERS

$$2d\sin\theta = p_1\lambda_1 = p_2\lambda_2 = ...$$

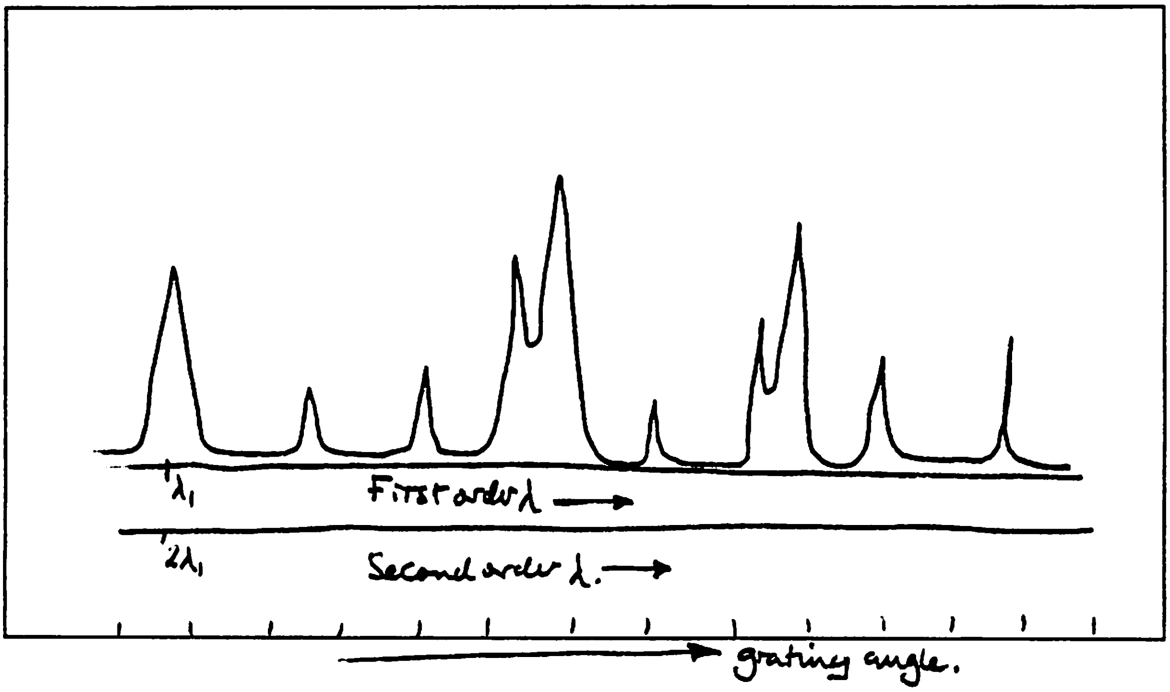

Use an order-sorter filter which absorbs the higher orders at shorter wavelengths.

STRAY LIGHT

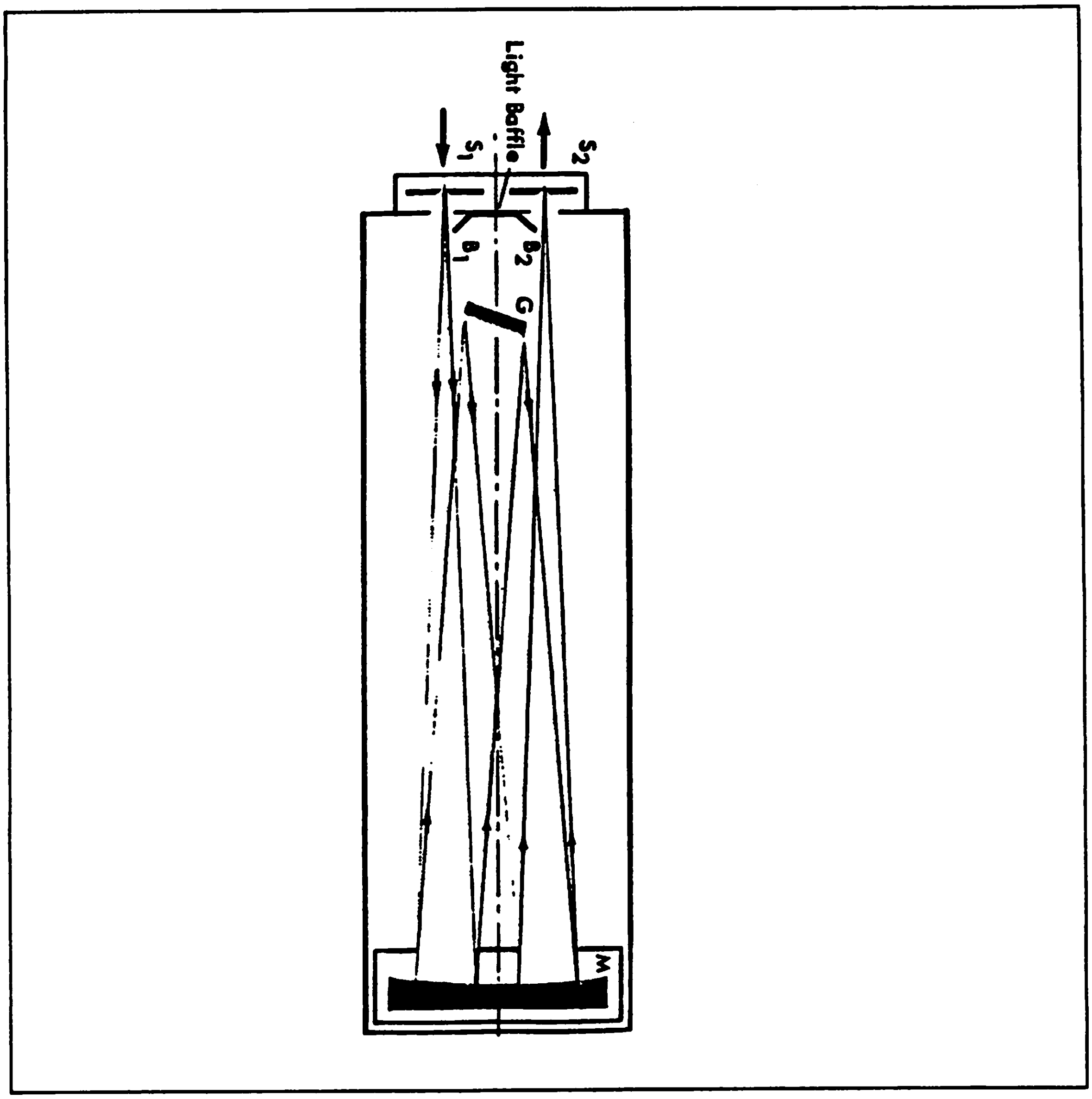

Dynamic Range of the Detector

Example: structure at the base of the 5577 line molecular oxygen first negative bands.

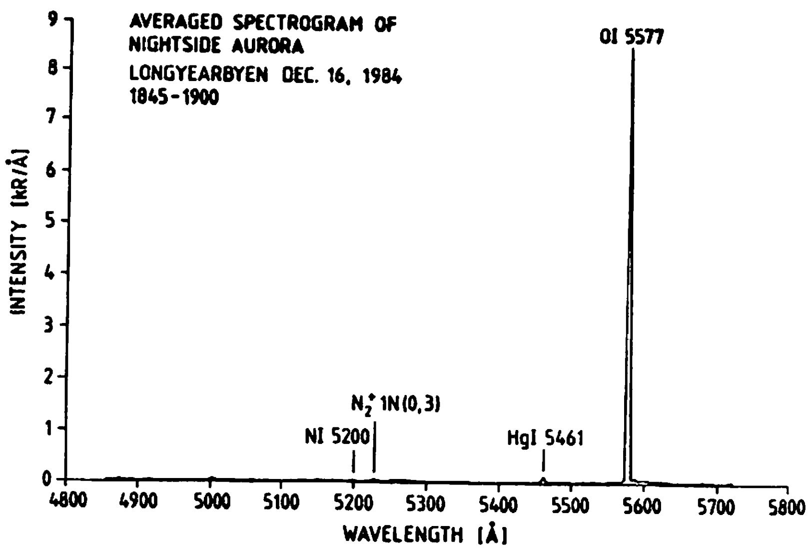

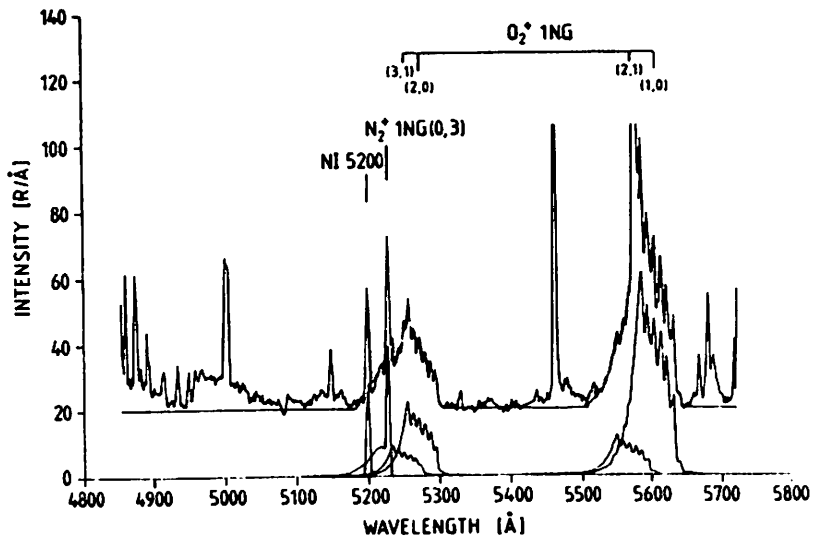

Michelson Interferometer

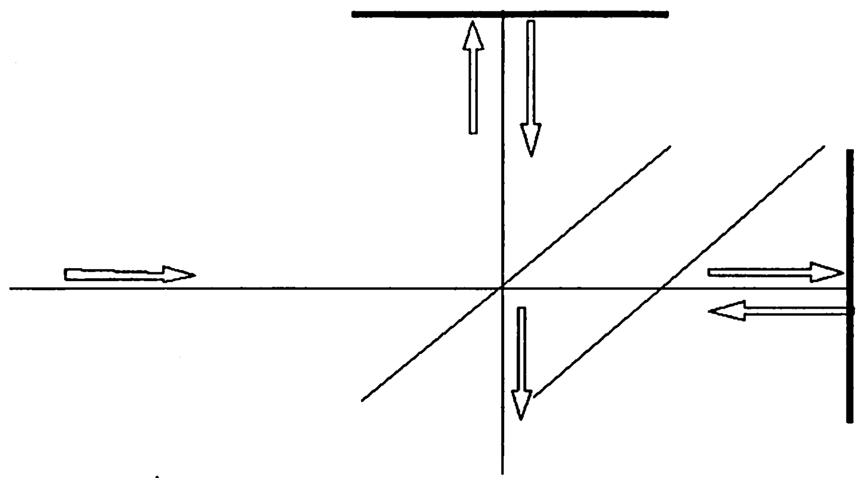

B(1 + cos(6.28sd)

s = wavenumber

d = path difference

Visibility = exp(- QTd^2)

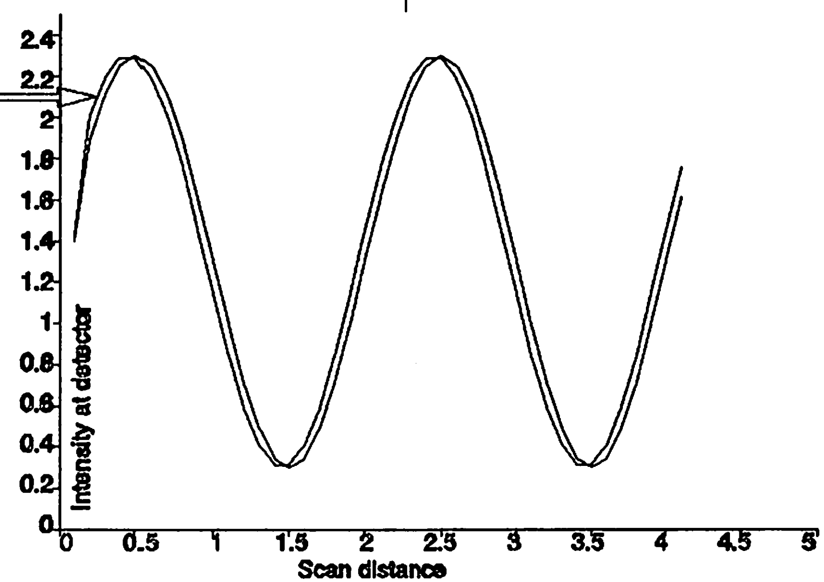

Fabry Perot Etalon

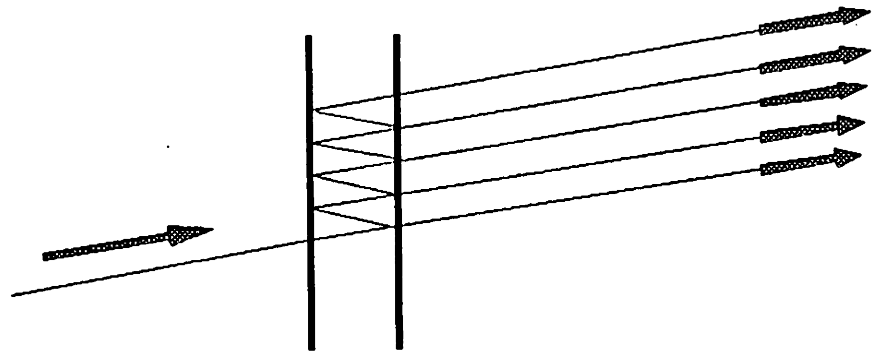

AT^2

Instrument Function

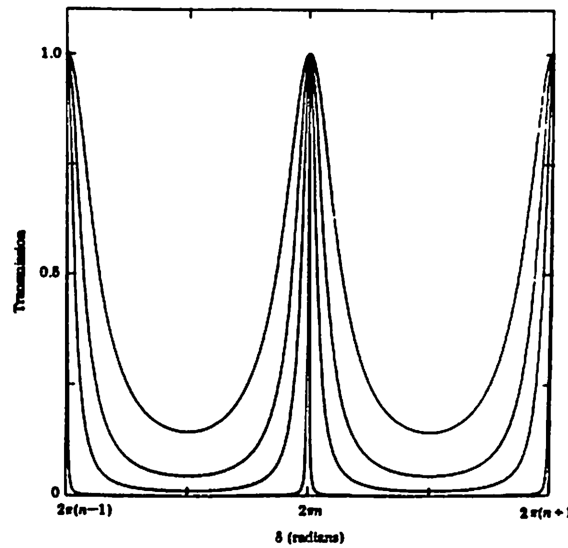

Sensitive to pressure (gas refractive index)
temperature
vibration

Field Widening for Michelson Interferometer

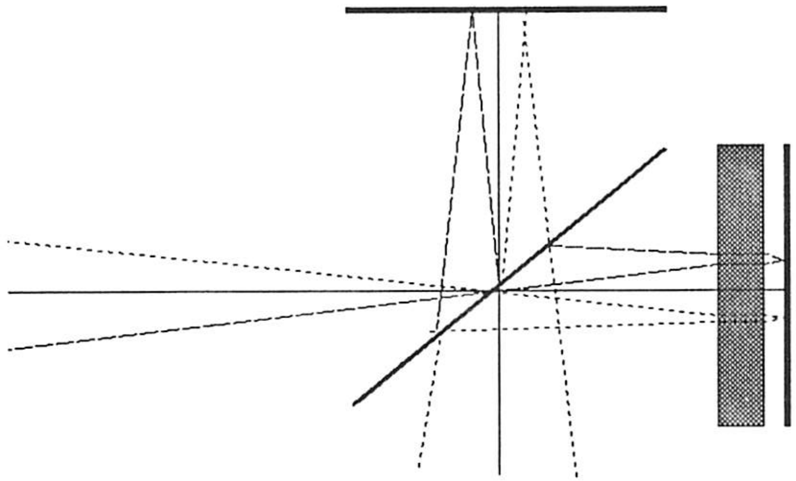

Maintains the quasi-zero path condition

→ when the path difference is non-zero

and the rays are off-axis

→ utilizing a glass block whose thickness is specific to the geometrical paths.

Field-Widening a Fabry-Perot Spectrometer

The Dual Etalon Modulator Approach

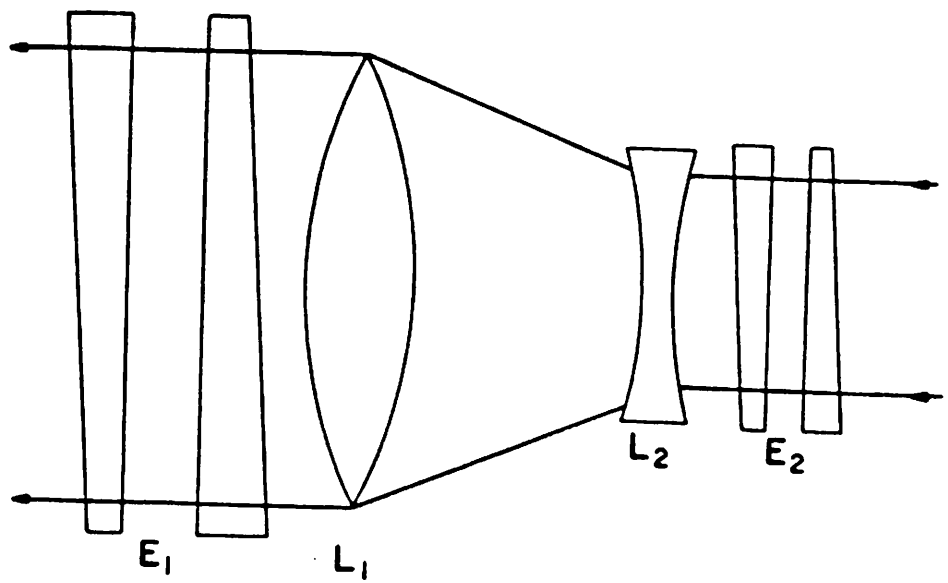

Fig. 1. Schematic representation of the beam expander used to couple the two etalons (E_1 and E_2) in this experiment.

FPI SCANNING

$$2nd\cos\theta = p\lambda$$

For pinhole scanning, θ may be considered close to zero and $\cos\theta = 1$

Hence $2nd = p\lambda$

Pressure scanning: p,d constant, vary n to scan λ
this is refractive index scanning

Piezo scanning: n,p constant, vary d to scan λ
this is scanning in plate separation

For spatial scanning, we may assume that θ is small so that
$\cos\theta = 1 - \theta^2/2$

Hence $\theta^2 = (p - p_0)/p_0$

where p_0 is the order at the center of the pattern.

Since θ is proportional to fringe radius, $p \alpha \text{ radius}^2$

Finding the peak wavelength of a profile

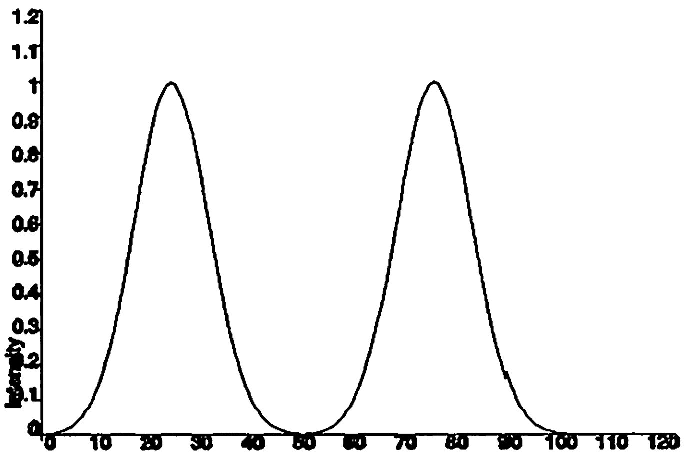

* Use a fit function

or

* Use the phase of FT

or

* Other suitable technique

For emissions not available in laboratory discharges

* get zero wavelength by averaging zenith

Scale velocities using standard Doppler theory.

Getting the Temperature from the spectrum

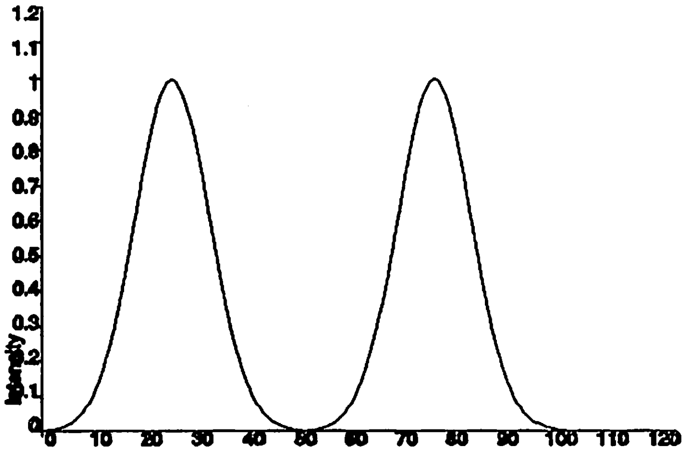

* Analyze using one FSR
* Remove instrument function
* Find best fit to Gaussian curve for T at given M.
* Check for Gaussian shape.